

# Theoretical analysis of long offset time-lapse frequency domain controlled source electromagnetic signals using the method of moments: Application to the monitoring of a land oil reservoir

C Schamper, Fayçal Rejiba, Alain Tabbagh, S Spitz

▶ **To cite this version:**

C Schamper, Fayçal Rejiba, Alain Tabbagh, S Spitz. Theoretical analysis of long offset time-lapse frequency domain controlled source electromagnetic signals using the method of moments: Application to the monitoring of a land oil reservoir. Journal of Geophysical Research : Solid Earth, 2011, 116 (B3), 10.1029/2009JB007114 . hal-01740100

**HAL Id: hal-01740100**

**https://normandie-univ.hal.science/hal-01740100**

Submitted on 17 Nov 2022

**HAL** is a multi-disciplinary open access archive for the deposit and dissemination of scientific research documents, whether they are published or not. The documents may come from teaching and research institutions in France or abroad, or from public or private research centers.

L'archive ouverte pluridisciplinaire **HAL**, est destinée au dépôt et à la diffusion de documents scientifiques de niveau recherche, publiés ou non, émanant des établissements d'enseignement et de recherche français ou étrangers, des laboratoires publics ou privés.

Copyright

# Theoretical analysis of long offset time-lapse frequency domain controlled source electromagnetic signals using the method of moments: Application to the monitoring of a land oil reservoir

C. Schamper,[1] F. Rejiba,[1] A. Tabbagh,[1] and S. Spitz[2]

Received 11 September 2009; revised 2 November 2010; accepted 27 December 2010; published 8 March 2011.

[1] We present a sensitivity study applied to water front monitoring of an onshore oil reservoir, using a remote controlled source electromagnetic method (CSEM) with electric dipoles and a borehole-to-surface configuration. We have developed an optimized and parallelized code based on the method of moments, in order to study the influence of several static or time-varying background uncertainties on the time-lapse CSEM signal (also called 4-D CSEM). Analysis of the relative and absolute variations in phase or quadrature of the time-lapse signal induced by the fluid substitution process, inside the reservoir, has shown that the vertical electric dipole allows the shape of the water front to be monitored, while remaining less sensitive (compared to a horizontal electric source dipole) to the total volume of substituted fluid. We have examined the influence of missed anomalies (1-D/3-D), with more or less conductive properties, near to the ground surface or the reservoir, and with or without time-varying properties. In most cases, the 4-D signal behaves like a reliable filter, canceling almost all response anomalies. However, it can also lead to strong, local perturbations of the time-lapse signal. We have also shown that in the presence of steel cased boreholes at the source location, or with outlying steel cased boreholes, the recording of exploitable data does not present insurmountable difficulties at low frequencies (~1 Hz), and for a dense array of surface receivers. These positive results with CSEM monitoring suggest that minimal, coarse-time 3-D explorations should be used to ensure reliable interpretation of the monitored data.

**Citation:** Schamper, C., F. Rejiba, A. Tabbagh, and S. Spitz (2011), Theoretical analysis of long offset time-lapse frequency domain controlled source electromagnetic signals using the method of moments: Application to the monitoring of a land oil reservoir, *J. Geophys. Res.*, *116*, B03101, doi:10.1029/2009JB007114.

## 1. Introduction

[2] The monitoring of reservoirs during production is implemented mainly to assess the efficiency and costs of recovery, and for security purposes to prevent the intrusion of water into the wells. Oil and gas production can induce essentially lateral displacements of the water-oil contact (WOC), because of the limited thickness of the reservoir, when compared with its lateral extent. The monitoring of an oil reservoir (i.e., WOC) requires the use of geophysical methods allowing the electrical conductivity contrast, associated with the boundary between oil and mineralized water, to be accurately discriminated.

[3] In order to tackle the problem of WOC monitoring, a numerical study based on controlled source electromagnetic (CSEM) methods is presented, for the case of the diffusive domain, i.e., the low-frequency domain in which there are no propagation phenomena. CSEM methods offer good sensitivity to the nature of the fluid, due to the electrical conductivity contrast between the oil-saturated and water-invaded parts of the reservoir. Despite their relatively low resolution (diffusive phenomena), they have become competitive with seismic methods (propagation phenomena), especially in compact and poorly fractured sediments such as carbonates, in which it is difficult for seismic techniques to distinguish between different fluids [*Wang et al.*, 1991; *Cadoret et al.*, 1995; *Wulff and Mjaaland*, 2002]. For further information concerning some of the initial time domain CSEM experiments, applied to petroleum exploration on land, the reader can refer to *Strack* [1992] and *Strack and Vozoff* [1996], who made use of long-offset transient electromagnetic (LOTEM). In order to first maximize the method's sensitivity to small WOC displacements, and secondly to ensure a reliable and stable source during the monitoring process, for a target located at a depth of 1 km, all of the simulations were made with a single vertical or horizontal electric source dipole situated inside the boreholes, associated with a dense grid of horizontal receiver dipoles located at the surface. Numerous studies dedicated to various specific contexts, with different geometrical scales and polarizations, converge toward the fact that the

[1]UMR 7619 Sisyphe, University Pierre and Marie Curie, Paris, France.
[2]CGGVeritas, Massy-Palaiseau, France.

Copyright 2011 by the American Geophysical Union.
0148-0227/11/2009JB007114

monitoring of resistivity variations should benefit from such an electric source/receiver configuration, especially at low frequencies, namely, below 10 Hz [*Newman*, 1994; *Pellerin and Hohmann*, 1995; *Liu et al.*, 2008; *He et al.*, 2005; *Hördt et al.*, 2000; *Wright et al.*, 2002]. The main current issues concern land CSEM applied to water-oil contact monitoring in the frequency domain, with potentially inadequate signal to noise levels, the source-receiver setup (type, overall positioning and polarization), shallow or near-reservoir 1-D and 3-D resistive or conductive anomalies, and, finally, steel casing effects. In practice, all of these factors lead to superimposed constructive or destructive interferences in the 4-D signal. The aim of the present paper is thus to study specific aspects of CSEM affected by these influences, for borehole-to-surface configurations using an electric source and electric receivers, at a frequency equal to 1 Hz.

[4] The issue of static or time varying background uncertainties is of major concern in many oil fields, and particularly when fine, thus costly, CSEM exploration has not been performed. As EM measurements in the low-frequency domain correspond to the integration of a large volume of the Earth surrounding the oil field, it can be expected that a poor knowledge of part of the subsurface, even far from the reservoir, could strongly modify the 4-D signal associated with the location at which fluid substitution occurs. A sensitivity study of offshore monitoring made by *Lien and Mannseth* [2008] shows that error cancellation of the misrepresentation of the background conductivity can be expected in the case of reasonable background conductivity errors. *Lien and Mannseth* [2008] showed that errors of nearly 10% in time-lapse signals are induced by a 50% overestimation of the conductivity of one of the following elements: a 200 m thick layer just below the seafloor, inside the entire background earth, or inside the oil reservoir, or a missed 40 m thick resistive layer just beyond the reservoir. In addition to the typical 1-D anomalies mentioned above, 3-D resistive heterogeneities associated with gas leakages and geochemical alterations may appear far above the reservoir [*Oehler and Sternberg*, 1984]. For the case of marine exploration, *Sasaki and Meju* [2009] have provided numerical evidence of galvanic effects on the 3-D signal of such resistive anomalies. On land, particular care has to be taken with near-surface changes of electrical conductivity, because frequent variations of water content can occur due to seasonal rainfall or drought. *Wirianto et al.* [2009] has analyzed this issue for a reservoir located at a depth of about 1.5 km, associated with variations in the near surface resistivity ranging between 10 and 50 Ω m. These results revealed that the latter variations produce a strong imprint, which does not however overwhelm the relative amplitude of the 4-D signal in the case of short offsets from the source (below 2 km), for surface-to-surface measurements. Therefore, in the case of a borehole-to-surface configuration at 1 Hz, we studied the influence of unnoticed thin conductive/resistive layers or 3-D bodies, which are alternatively located near to the surface and just above the oil reservoir. In addition, by using a buried VED (Vertical Electric Dipole) source and HED (Horizontal Electric Dipole) surface receivers at 1 Hz, the time-lapse signals were calculated for the case of a strongly time-varying conductivity, ranging from 0.01 to 1 S/m between two measurements.

[5] The final issue, and perhaps the most challenging from a numerical point of view, is related to the impact of a steel casing located at the borehole used for the CSEM monitoring, and of an outlying steel casing. The majority of reservoir boreholes are surrounded by a steel casing which, theoretically, should not prevent the diffusion of EM waves at very low frequencies. An early study published by *Augustin et al.* [1989] reported very good sensitivity to the measurement, through the steel casing, of the surrounding conductivity at low frequencies and for a surface-to-borehole device. However, they studied the EM field measured inside the cased borehole, using a large-loop transmitter located on the surface. *Kong et al.* [2009] have recently proposed a very interesting study of EM field diffusion with an electric dipole located inside a cased borehole, which shows how the steel casing is energized. This work, inspired by *Kaufman* [1990], is based on the replacement of the energized steel casing by a series of equivalent vertical dipole sources with decreasing intensities. As the modeling of a very fine structure for long-offset measurements leads to significant difficulties, whatever the modeling method used, we used the same source-equivalence approach to study the effect of centered, cased boreholes (at the source location). For outlying cased boreholes, the steel casing was modeled as a highly conductive 3-D heterogeneity.

[6] An optimized (using the Toeplitz matrix formalism) and parallelized (EM_MOM) code, using the method of moments, has been developed to investigate the issues highlighted above [*Schamper*, 2009]. In particular, we studied the influence of several heterogeneities (1-D, 3-D, casing, time varying properties) on the land 4-D-CSEM forward response, for a large-scale problem and for an electric configuration involving a buried VED (or HED) associated with a dense grid of HED receivers on the surface, at a single frequency equal to 1 Hz.

## 2. Methodological Development

[7] As we are interested in the time-lapse response of a zone limited to a reservoir and its neighborhood, the semi-analytical and so-called method of moments (MoM) modeling, described for electrical conductivity contrast several decades ago by *Wait* [1966] and *Hohmann* [1975], is an interesting approach for the purposes of our theoretical study of CSEM monitoring. It enables discretization of the 3-D domain only, representing the target, and for which the numerical electromagnetic response is superposed onto the analytical solution of a tabular Earth (see the Green function from *Wannamaker et al.* [1984]). Recent improvements made by *Zhdanov* [2002] allow more complex and larger models to be built using this method.

[8] The superposition of the tabular Earth and 3-D body responses can first be summarized by

$$\boldsymbol{E} = \boldsymbol{E_b} + \boldsymbol{E_s} \tag{1}$$

where $\boldsymbol{E}$ is the total electric field, $\boldsymbol{E_b}$ is the background electric field associated with a simplified "1-D Earth," and $\boldsymbol{E_s}$ is the scattering field due to the presence of a 3-D heterogeneity in the electrical conductivity. The particularity of

this method is that it requires discretization of the 3-D space only in the zone of the heterogeneity. Its electromagnetic response will be proportional to the difference between the conductivities of the 3-D body and the background, as can be seen in the integral development of equation (1) [*Hohmann*, 1975]:

$$\boldsymbol{E}(\boldsymbol{r_{rec}}) = \boldsymbol{E_b}(\boldsymbol{r_{rec}}) + \int_V \boldsymbol{G_{EJ}}(\boldsymbol{r_{rec}}, \boldsymbol{r'}) \cdot \delta\widetilde{\sigma}(\boldsymbol{r'})\boldsymbol{E}(\boldsymbol{r'})dr' \quad (2)$$

where $\boldsymbol{r_{rec}}$ is the position of the receiver, $V$ is the volume of the 3-D heterogeneity, $\boldsymbol{r'}$ is the position of a unit source inside the 3-D body, $\boldsymbol{G_{EJ}}(\boldsymbol{r}, \boldsymbol{r'})$ is the analytical Green function [3 × 3], here for a tabular Earth (i.e., with resistivity variations along the vertical axis only), which expresses the electric field at position $\boldsymbol{r}$ for a unit electric dipole at position $\boldsymbol{r'}$, and $\delta\widetilde{\sigma}$ is the difference in conductivity between the 3-D body and the background.

[9] It is important to note that we should thus always reason in terms of conductivity differences (S/m), rather than resistivity ratios. Actually, a highly resistive body located inside a relatively resistive environment (e.g., 500 to 50 Ω m) will have a poor response, even though the resistivity ratio between these two components may be quite high. In the present study, we expect a notable response due to the large difference in conductivity between rocks containing brine (about 1 S/m) and rocks containing a high proportion of oil (about 0.01 S/m).

[10] For the purposes of computing the volume integral of equation (2), the heterogeneity domain is discretized into rectangular parallelepipeds, which are sufficiently small in comparison with the wavelength of the source frequency: $L \ll |1/k|$. This condition allows the electric field to be considered as constant inside each cell [*Tabbagh*, 1985]. Because of the low frequencies used in oil CSEM methods, i.e., around 1 Hz, the lateral size of the cells often lies in the range between 50 and 100 m. Inside the 3-D body, equation (2) becomes

$$\boldsymbol{E}(\boldsymbol{r_i}) - \sum_{k=1}^{N}\left[\delta\widetilde{\sigma}(\boldsymbol{r_k})\boldsymbol{E}(\boldsymbol{r_k}) \cdot \int_{V_k} \boldsymbol{G_{EJ}}(\boldsymbol{r_i}, \boldsymbol{r'})dr'\right] = \boldsymbol{E_b}(\boldsymbol{r_i}) \quad \forall\ \mathrm{i} \in (1, \mathrm{N}) \quad (3)$$

where $\boldsymbol{r_i}$ are the coordinates of the center of the $i$th cell, $N$ is the number of cells from which the 3-D heterogeneity is composed, $k$ is the index corresponding to one of the $N$ cells, and $V_k$ is the volume of the $k$th cell.

[11] If the total electric field is defined as the sum of a primary field and a secondary (or scattered) field, as expressed in equation (1), then equation (3) can be written for the scattered field only:

$$\boldsymbol{E_s}(\boldsymbol{r_i}) - \sum_{k=1}^{N}\left[\delta\widetilde{\sigma}(\boldsymbol{r_k})\boldsymbol{E_s}(\boldsymbol{r_k}) \cdot \int_{V_k} \boldsymbol{G_{EJ}}(\boldsymbol{r_i}, \boldsymbol{r'})dr'\right] = \sum_{k=1}^{N}\left[\delta\widetilde{\sigma}(\boldsymbol{r_k})\boldsymbol{E_b}(\boldsymbol{r_k}) \cdot \int_{V_k} \boldsymbol{G_{EJ}}(\boldsymbol{r_i}, \boldsymbol{r'})dr'\right] \forall\ \mathrm{i} \in (1, \mathrm{N}) \quad (4)$$

Equation (4) is the central part of the method of moments and needs to be handled with care in order for its computation to be well optimized. The analytic Green function needs to be computed first, which is time consuming due to the numerical computation of the Hankel transform [*Guptasarma and Singh*, 1997]. Although the number of cell interactions ($N^2$) increases rapidly, there are several computational tricks which can be used to reduce the computation time. Diffusion of the electromagnetic field at low frequencies allows interpolation methods, such as the cubic spline, to be used effectively to reduce the number of calls to the Green function itself. Since the Green function is used to represent a horizontally layered Earth, rotation about the vertical axis can be used to fill the electromagnetic interaction matrix.

[12] Equation (4) is a square linear system [$3N$, $3N$] with the electric fields inside each cell being the unknowns ($3N$). The latter system is not sparse, and its solution is computationally challenging when the number of cells is large. Due to the axial symmetry of the tabular Earth, the electromagnetic dependence matrix (corresponding to the electromagnetic interactions between the cells of the 3-D heterogeneity) has a two-dimensional Toeplitz structure, which allows the matrix-vector operation to be accelerated inside an iterative solver [*Barrowes et al.*, 2001]. Recent improvements in the solving of linear systems, and the increasing availability of distributed computational resources, allow the response of a relatively complex model based on this technique to be computed, by solving the entire system. Various approximations have been proposed, such as the Born, the Quasi-Analytical [*Zhdanov et al.*, 2000a], and the Quasi Linear [*Zhdanov et al.*, 2000b] methods, to avoid solving the complete system. These allow millions of cells to be managed, thus making it possible to compute the field over very large scales. In the present study, we chose not to analyze the accuracy of these approximations, but rather to focus on the results themselves, by solving the full integral equation.

[13] Once the electric field has been computed inside each cell, the electromagnetic field can be deduced everywhere, using the following equation:

$$\boldsymbol{E}(\boldsymbol{r_{rec}}) = \boldsymbol{E_b}(\boldsymbol{r_{rec}}) + \sum_{k=1}^{N}\left[\delta\widetilde{\sigma}(\boldsymbol{r_k})\boldsymbol{E}(\boldsymbol{r_k}) \cdot \int_{V_k} \boldsymbol{G_{EJ}}(\boldsymbol{r_{rec}}, \boldsymbol{r'})dr'\right]. \quad (5)$$

[14] In this paper, we have adapted the equations described in detail by *Lien and Mannseth* [2008] with our own notations, in order to highlight the impact of a background error on the 4-D signal inside the integral equations. First, the 3-D measurement error can be expressed as

$$\begin{aligned}\boldsymbol{E}^{\mathbf{tab_2}}(\boldsymbol{r_{rec}}) - \boldsymbol{E}^{\mathbf{tab_1}}(\boldsymbol{r_{rec}}) &= \boldsymbol{E_b}^{\mathbf{tab_2}}(\boldsymbol{r_{rec}}) - \boldsymbol{E_b}^{\mathbf{tab_1}}(\boldsymbol{r_{rec}}) \\ &+ \sum_{k=1}^{N}\left[\delta\widetilde{\sigma}_k\left(\boldsymbol{E}^{\mathbf{tab_2}}(\boldsymbol{r_k}) \cdot \int_{V_k} \boldsymbol{G}_{\boldsymbol{EJ}}^{\mathbf{tab_2}}(\boldsymbol{r_{rec}}, \boldsymbol{r'})dr'\right.\right. \\ &\left.\left. -\boldsymbol{E}^{\mathbf{tab_1}}(\boldsymbol{r_k}) \cdot \int_{V_k} \boldsymbol{G}_{\boldsymbol{EJ}}^{\mathbf{tab_1}}(\boldsymbol{r_{rec}}, \boldsymbol{r'})dr'\right)\right] \end{aligned} \quad (6)$$

where the subscripts $\mathrm{tab_2}$ and $\mathrm{tab_1}$ correspond to two different tabular backgrounds.

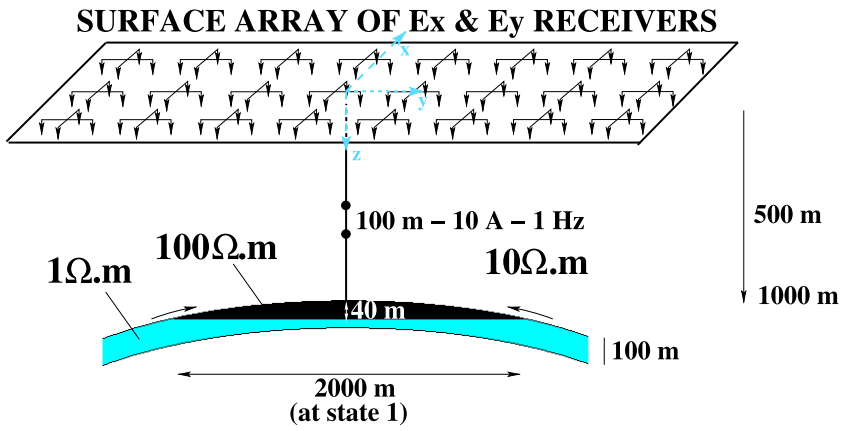



**Figure 1.** A 3-D dome hydrocarbon reservoir, with oil in the upper zone (0.01 S/m) having an initial lateral extent of 2000 m. The slope has a maximum low dip of 3°. Water-invaded zone below the oil: 1 S/m. Vertical electric dipole at a depth of 500 m, with a 100 m electrode spacing, a current of 10 A, and a frequency of 1 Hz. Electric and magnetic receivers are arranged on the Earth.

[15] If it can be assumed that the background does not change between two states, then the time-lapse signal of the reservoir can be written as

$$\boldsymbol{E}^{t_2}(\boldsymbol{r}_{rec}) - \boldsymbol{E}^{t_1}(\boldsymbol{r}_{rec}) = \sum_{k=1}^{N}\left[\int_{V_k} \boldsymbol{G}_{EJ}(\boldsymbol{r}_{rec},\boldsymbol{r}')d\boldsymbol{r}' \cdot \left(\delta\widetilde{\sigma}_k^{t_2}\boldsymbol{E}^{t_2}(\boldsymbol{r}_k) - \delta\widetilde{\sigma}_k^{t_1}\boldsymbol{E}^{t_1}(\boldsymbol{r}_k)\right)\right] \quad (7)$$

where the subscripts $t_2$ and $t_1$ correspond to two different times, or states of the monitored reservoir.

[16] As can be seen in equation (6), additional and non-negligible errors can arise from $\boldsymbol{E}_b^{\mathbf{tab}_2}(\boldsymbol{r}_{rec}) - \boldsymbol{E}_b^{\mathbf{tab}_1}(\boldsymbol{r}_{rec})$, which is cancelled by applying a time difference to the total field of the 3-D measurements, in order to obtain the 4-D data of equation (7). The total electric field inside each cell can be separated into two terms, written as: $\boldsymbol{E}^{t_i}(\boldsymbol{r}_k) = \boldsymbol{E}_b(\boldsymbol{r}_k) + \boldsymbol{E}_s^{t_i}(\boldsymbol{r}_k)$. Equation (7) then becomes

$$\begin{aligned}\boldsymbol{E}^{t_2}(\boldsymbol{r}_{rec}) - \boldsymbol{E}^{t_1}(\boldsymbol{r}_{rec}) &= \sum_{k=1}^{N_{fixed}}\left[\int_{V_k} \boldsymbol{G}_{EJ}(\boldsymbol{r}_{rec},\boldsymbol{r}')d\boldsymbol{r}' \cdot \delta\widetilde{\sigma}_k\left(\boldsymbol{E}_s^{t_2}(\boldsymbol{r}_k) - \boldsymbol{E}_s^{t_1}(\boldsymbol{r}_k)\right)\right] \\ &+ \sum_{k=1}^{N_{changed}}\left[\int_{V_k} \boldsymbol{G}_{EJ}(\boldsymbol{r}_{rec},\boldsymbol{r}')d\boldsymbol{r}' \cdot \left[\boldsymbol{E}_b(\boldsymbol{r}_k)\left(\delta\widetilde{\sigma}_k^{t_2} - \delta\widetilde{\sigma}_k^{t_1}\right)\right.\right. \\ &\left.\left. + \left(\delta\widetilde{\sigma}_k^{t_2}\boldsymbol{E}_s^{t_2}(\boldsymbol{r}_k) - \delta\widetilde{\sigma}_k^{t_1}\boldsymbol{E}_s^{t_1}(\boldsymbol{r}_k)\right)\right]\right] \quad (8)\end{aligned}$$

where $N_{fixed}$ is the number of cells in which the conductivity has not changed, from time $t_1$ to time $t_2$, and $N_{changed}$ is the number of cells in which the conductivity has changed from time $t_1$ to time $t_2$ by fluid replacement.

[17] The time-lapse signal is proportional to the background field, only in the zone where the oil saturation changes ($N_{changed}$). This region has a volume which is smaller than the total volume of the 3-D target. Therefore, the effect of a poorly known background could be attenuated. As equation (4) clearly indicates that there is no simple relationship between the scattered ($\boldsymbol{E}_s$) and background ($\boldsymbol{E}_b$) fields, which can be extracted from the full linear system, additional numerical analysis is required to precisely quantify the impact of a poorly known background on the 4-D signal.

## 3. Borehole-to-Surface 4-D Response: HED Versus VED Configuration

[18] In this study, we compare the responses resulting from both a horizontal (HED) and a vertical electric dipole (VED) source. Previous works by *Newman* [1994] and *Pellerin and Hohmann* [1995] have considered the case of a buried vertical electric source. *Newman* [1994] considered both cross-well and borehole-to-surface measurements. For the latter configuration, the EM monitoring of an EOR (Enhanced Oil Recovery) process was simulated very near to the surface (around 20 m depth). In the present paper, the EM device must be capable of monitoring the water front over surface areas of the order of several square kilometers, for a target located at a depth of 1 km. *Newman* [1994]

**Table 1.** Different States of the 3-D Oil Reservoir

| State | Average Oil Recovered[a] (Mbbl) | Rock Volume Containing Oil ($Mm^3$) | Top Surface of Oil Disc ($km^2$) | Diameter of Top Surface (m) | Maximum Thickness of Oil Disc (m) |
|---|---|---|---|---|---|
| 1 | 30.04 | 79.6 | 3.76 | 2200 | 40 |
| 2 | 22.30 | 60.8 | 3.32 | 2000 | 35 |
| 3 | 16.68 | 44.2 | 2.76 | 1800 | 30 |
| 4 | 11.47 | 30.4 | 2.16 | 1600 | 25 |
| 5 | 7.40 | 19.6 | 1.72 | 1400 | 20 |
| 6 | 4.15 | 11.0 | 1.20 | 1200 | 15 |
| 7 | 1.89 | 5.0 | 0.76 | 1000 | 10 |
| 8 | 0.45 | 1.2 | 0.24 | 800 | 5 |

[a]Mbbl, one million barrels.

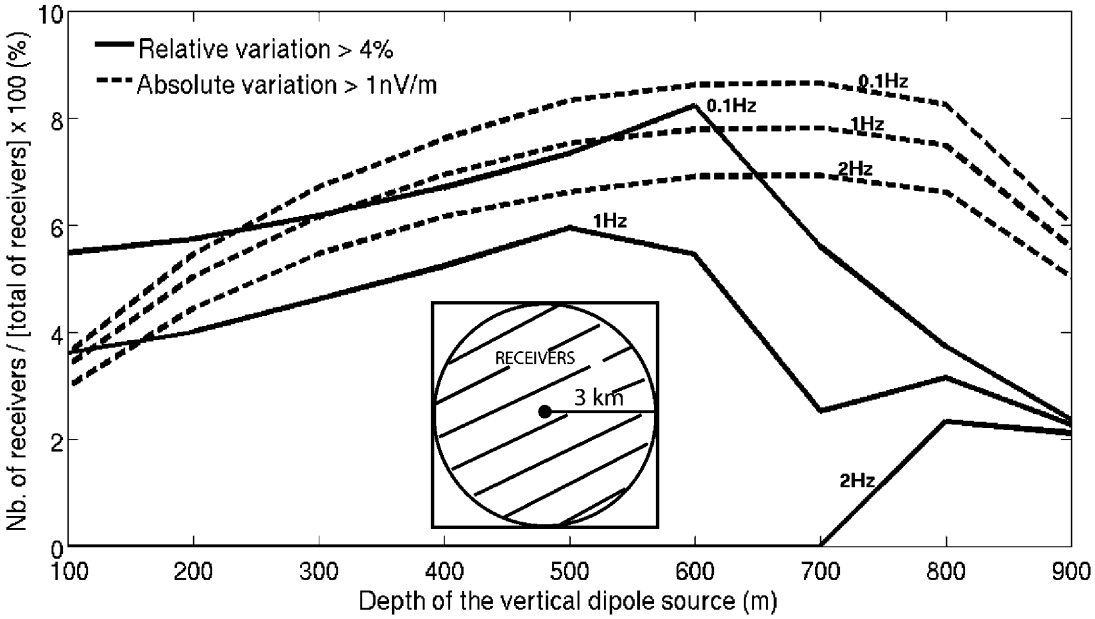



**Figure 2.** Number of receivers (Ex component) for which the relative variation in amplitude is greater than 4% (solid lines) and for which the 4-D amplitude signal is stronger than 1 nV/m (dashed lines). Time-lapse signal between states 1 and 3 (3vs1, compare Table 1). Variation as a function of the depth of a vertical electric dipole (10 A, 100 m). All of the receivers are arranged on the Earth's surface, within a radius of 3 km centered on the borehole containing the source.

noted that the inductive response is better if a VED is considered, rather than a VMD (Vertical Magnetic Dipole), for which the response drops off rapidly at low frequencies. Newman worked at frequencies above 500 Hz, which suggests that a VMD should not be considered in our case, since our measurements are made at a frequency close to 1 Hz. Contrary to *Newman* [1994], who was particularly interested in the magnetic components at the receiver locations, we present here the measurements of the electric field components only. *Pellerin and Hohmann* [1995] focused their parametric study of a VED source on the characterization of a mineral target which was more conductive than the background, and located at a depth around 500 m. In the present study, we focused on the monitoring of a deep oil reservoir, which is more resistive than the surroundings. As in the work by *Newman* [1994], *Pellerin and Hohmann* [1995] focused more closely on the magnetic field, on the vertical component

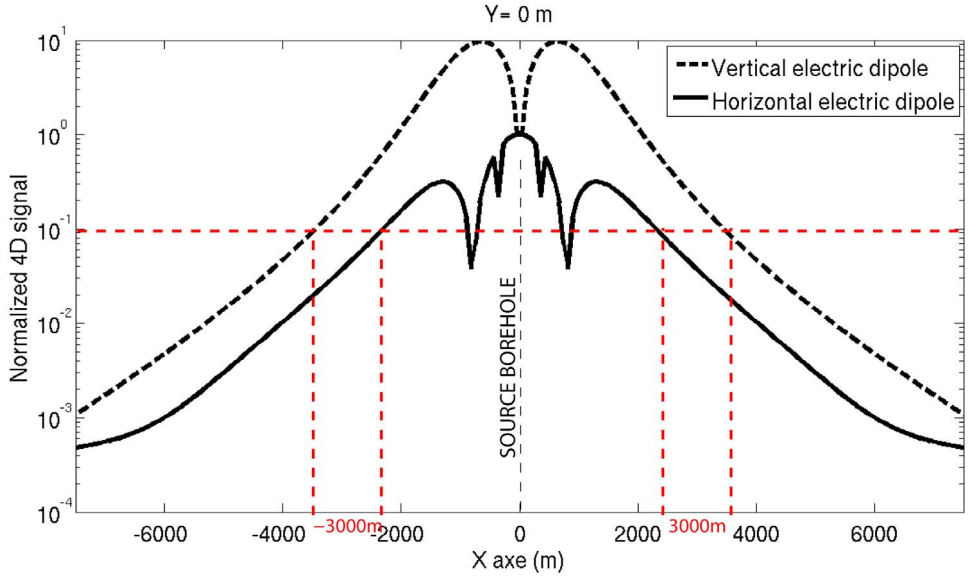



**Figure 3.** Normalized 4-D signal of the Ex component, between the reservoir's states 1 and 3. Buried vertical or horizontal electric dipole at 1 Hz (100 m, 10 A). Profile $Y = 0$ m.

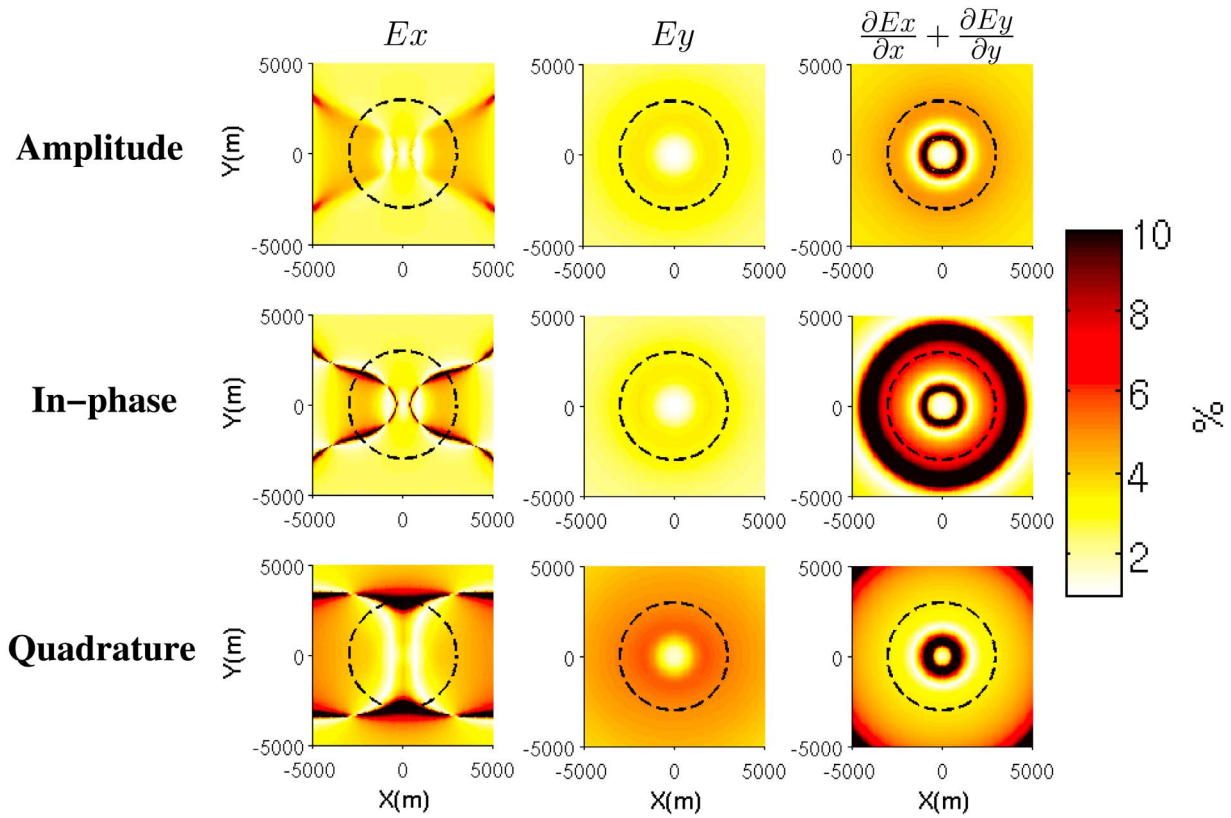



**Figure 4.** Relative variations (amplitude, in-phase, and quadrature components) for a deep horizontal electric dipole (100 m, 10 A, 1 Hz) between states 1 and 3 of the reservoir (dashed line indicates circle of 3 km radius).

in particular, which is nonexistent in the case of a 1-D Earth with a VED, and which may highlight the presence of a 2-D/3-D structure. Here, we concentrate our analysis on the electric field components of time-lapse signals.

[19] Two criteria need to be observed in order to carry out this theoretical study. First, the relative amplitude variations of the CSEM signal have to be greater than a few percent. According to previous studies, we set the lower limit to 1% [*Hördt et al.*, 2000; *Orange et al.*, 2009]. A time-lapse signal is then considered to be nonexistent below this threshold. It is reasonable to attempt to go down to this level, since numerous stacks can be made during the monitoring measurements. Second, it is essential to check the amplitude variation itself. Even though a significant relative variation may be found with the numerical simulations, the amplitude variation could be far below the sensitivity of the best geophysical sensors. For the electric field, the lower limit is set to 1 nV/m, which gives a limit of 10–100 nV for a 10–100 m long receiver. This level was defined via passive measurements of the electric field, made in Arpajon (30 km southwest of Paris) by CGGVeritas. The noise level reached after 2–3 days of vertical stacking was below 100 nV for copper electrodes separated by 100 m.

[20] *Schamper et al.* [2008] proposed an oil reservoir model, which we made more complex by adding a slope to the reservoir (Figure 1). The oil is pumped from the cap of a domed structure, which has a dip around 3°, such that a 100 m lateral displacement of the WOC corresponds to a rise of 5 m. The top of the vertical-axis-symmetric dome is located 1000 m beneath the surface. For the background Earth, we set the conductivity to 0.1 S/m, which is a high value on land. This does not make it easy to achieve good resolution of the reservoir edges, since low-frequency emission is necessary to reach the target (in our case, the 4-D CSEM signal is essentially due to the replacement of the oil, 0.01 S/m, by conductive mineralized water, 1 S/m). Mineralized and highly conductive water is located below the oil-saturated part of the reservoir, for which the conductivity is set to 0.01 S/m. The high conductivity of the water-invaded part of the reservoir, set to 1 S/m, i.e., close to the conductivity of marine sediments, should provide a sensitive EM response to the WOC.

[21] Details of several states of the reservoir are enumerated in Table 1. Table 1 gives the numbers we use to designate the different states of the oil reservoir production, the number of potentially produced barrels, assuming a porosity of 30% and an oil recovery rate of 20%, the rock volume is directly related to average oil recovered, since it corresponds to the volume of rock, which is highly saturated with oil. The oil reservoir has a domed structure whose vertical section can be seen in Figure 1. The upper part, which is saturated with oil, forms a disc in the top view. The upper surface area of this disc and its diameter are given in Table 1. Table 1 also gives the maximum thickness of the oil disc located at the vertical axis of symmetry of the reservoir. For the oil disc diameter in

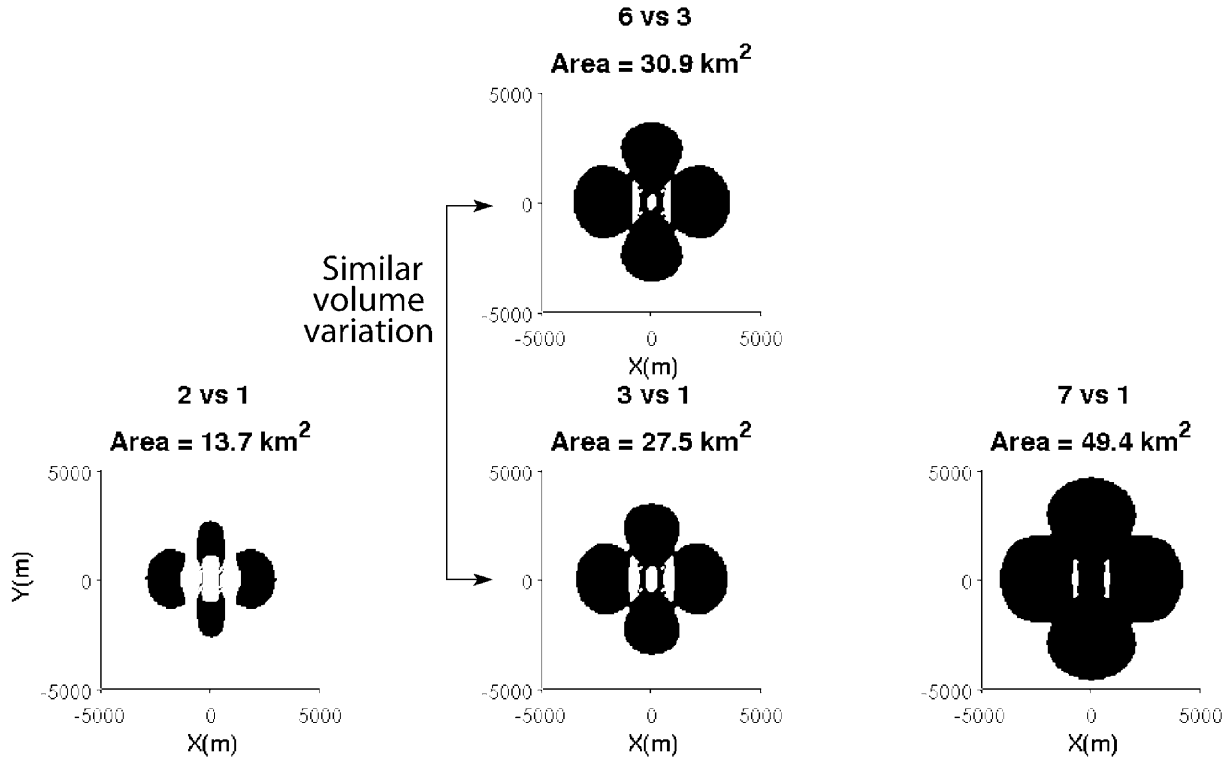



**Figure 5.** Measurable zone of the Ex component for a deep horizontal electric dipole (100 m, 10 A, 1 Hz). Conditions are as follows: Relative amplitude variations >1% and absolute amplitude variations >1 nV/m. The variations are based on a comparison with the initial state 1 of the reservoir. The step from state 3 to state 6 (indicated by 6vs3) has been added for comparison with the step from state 1 to state 3, which corresponds to a similar volume of fluid substitution.

Table 1, between two consecutive states, the WOC is displaced by 100 m from the periphery. The maximum thickness of the oil disc shows that the water level rises by 5 m between each step. As can be noticed, the evolution of the volume of fluid substitution is not linear. The last states of the reservoir in this table correspond to the smallest volumes of fluid replacement. In the following, we consider the evolution of the oil reservoir, from state 1 to 3, as the reference step. This step will be designated as 3vs1. Since we are more interested in the lateral displacement of the WOC than in the estimation of the quantity of oil, we chose to make a specific investigation of the smallest fluid substitutions, in an attempt to test the EM device's ability to follow the lateral movement, despite the smaller volume of change in conductivity.

[22] Since surface-to-surface land CSEM monitoring has not previously led to very conclusive results [*Strack et al.*, 2009], it was decided to bury the electric source to enhance the signal-to-noise ratio of the time-lapse data. In order to increase the measurement system's sensitivity to the lateral extent of the reservoir, we chose to install a very dense array of receivers at the surface. Since the source is buried deep in a borehole (two boreholes in the case of a horizontal, two-electrode dipole), it is not possible to use the in-line electric field generated by a horizontal electric dipole, towed with a constant offset between the source and the receiver. This configuration has demonstrated good sensitivity to a thin resistive layer, with broadside data assisting with the retrieval of information relevant to the global Earth model. This was verified by *Eidesmo et al.* [2002], who also underlined the strong effect of a thin resistive layer on the vertical component of the electric current. However, the vertical electric component, Ez, has a very weak amplitude ($10^5$ times smaller than the horizontal components) near to the Earth's surface. For the case of shallow water (100 m), which is similar to the case of land, *Andréis and MacGregor* [2008] have shown that isolating the Transverse Magnetic (TM) mode (a method described by *Andréis* [2008]), which contains the Ez component (Hz being zero), helps in obtaining a high sensitivity, similarly to when the Ez component is measured directly. Gauss' law, with no chargeability, leads to

$$\nabla . \boldsymbol{E} = \frac{\rho}{\epsilon_0} \Rightarrow \nabla . \boldsymbol{E} \approx 0 \tag{9}$$

where $\rho$ is the charge density (C/m$^3$) and $\epsilon_0$ is the electric permittivity of free space (F/m).

[23] Equation (9) leads to the following:

$$\frac{\partial E_z}{\partial z} \approx -\left(\frac{\partial E_x}{\partial x} + \frac{\partial E_y}{\partial y}\right) \tag{10}$$

Expression (10) will be used in the following sensitivity study to compute $\partial Ez/\partial z$ from the measured values of the horizontal components.

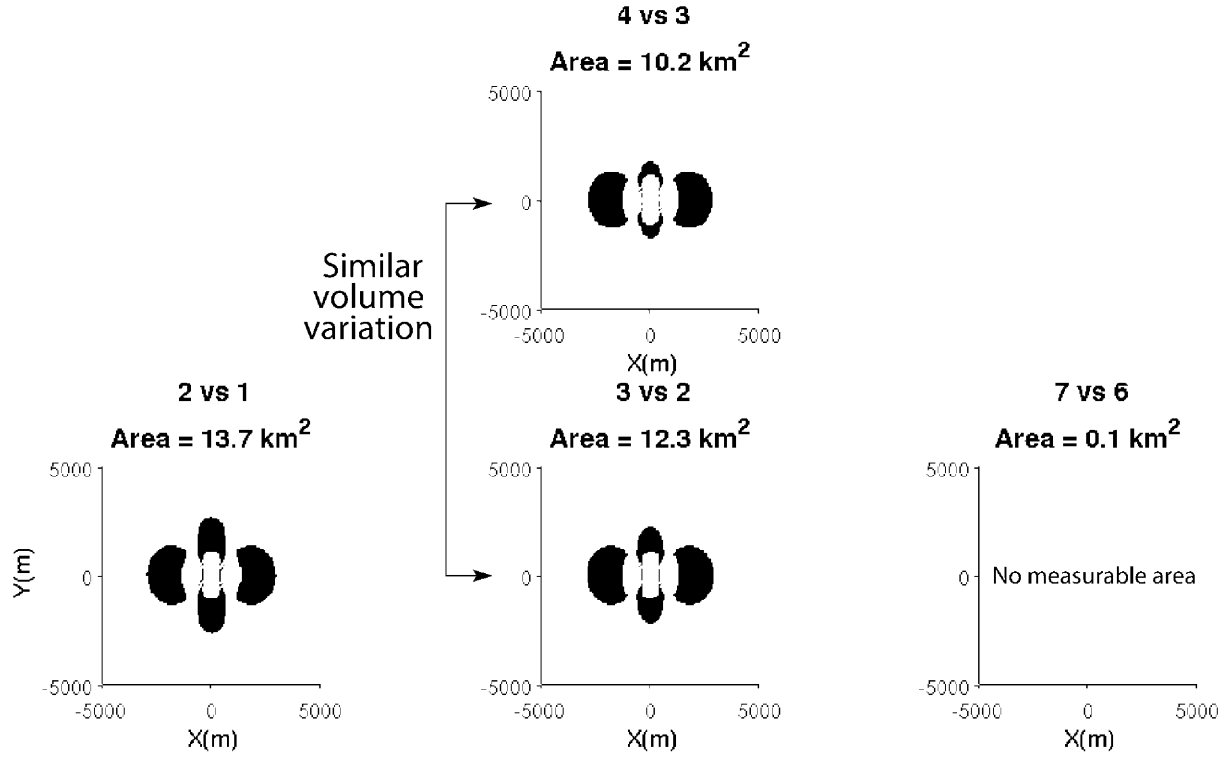



**Figure 6.** Measurable zone of the Ex component, for a deep horizontal electric dipole (100 m, 10 A, 1 Hz). Conditions are as follows: Relative amplitude variations >1% and absolute amplitude variations >1 nV/m. The variations represented here are with respect to the previous state (i-1) of the reservoir. The graph showing the step from state 3 to state 4 has been added for the purposes of comparison with the step from state 2 to state 3, which corresponds to a similar volume of fluid substitution.

[24] It is necessary to determine the optimal depth and frequency of the vertical dipole source in order to enhance the 4-D reservoir signal. For this purpose, simulations were made by varying both the depth and the frequency of the electric source. Figure 2 plots the change in the number of receivers for which there is a notable change in terms of relative variation, and in terms of absolute amplitude variation as a function of the depth of the vertical dipole source, over the frequency range 0.1–2 Hz. The number of receivers is expressed in percent and corresponds to the proportion of the surface of a 3 km radius circle, in which all receivers are equally spaced. A depth of 500 m, at middistance between the receivers and the target, seems to be a good choice. In fact there is a drop in the time-lapse signal shortly beyond this depth. This can be explained by the fact that the vertical electric dipole generates essentially vertical electric currents. As a consequence of the source geometry, these vertical currents lead to a considerably weaker irradiation of the far-from-borehole water front, as long as the source is close to the center of the reservoir. Another cause of the decrease in number of sensitive receivers (where relative and absolute variations are larger than 4% and 1 nV/m, respectively) is the fact that the 4-D information tends to be more concentrated near to the surface of the Earth, when the source is closer to the depth of the monitored target. Inversely, the closer the source is brought to the surface, the greater the lateral offset required in order for the energy maximum of the time-lapse signal to be recorded. In the particular case of surface-to-surface measurements, the optimal offset is around 2–5 times the depth of the target, depending on the frequency and the conductivity of the Earth. With respect to frequency, there is a slight decrease between 0.1 and 1 Hz, whereas between 1 and 2 Hz the number of receivers above 4% drops dramatically. This can be explained by the skin depth (or depth of penetration) of the electromagnetic signal, which decreases when the frequency increases. A frequency of 1 Hz was retained for the following simulations.

[25] In Figures 4–11, the results are presented on a 10 km by 10 km surface array centered on the source borehole. Figure 3 shows the 4-D signal of Ex along the profile $Y$ = 0 m, for buried vertical (dashed line) and horizontal (solid line) electric dipoles, between states 1 and 3 of the reservoir (see Table 1). The time-lapse response is normalized by the 4-D signal measured just above the borehole. As can be seen (Figure 3), the time-lapse signal remains at a maximum value inside a radius of less than 1 km. It reaches 10 times the amplitude above the borehole for a vertical dipole, and a local maximum ($X \approx \pm 1200$ m) 7–8 times smaller than the field measured above the source for the horizontal electric dipole. Comments concerning the relative variations will be relevant for our case, inside a radius of no more than 3 km. Beyond this radius, the time-lapse signal is 100 times smaller than its maximum amplitude for the vertical dipole and 10 times smaller for the horizontal one.

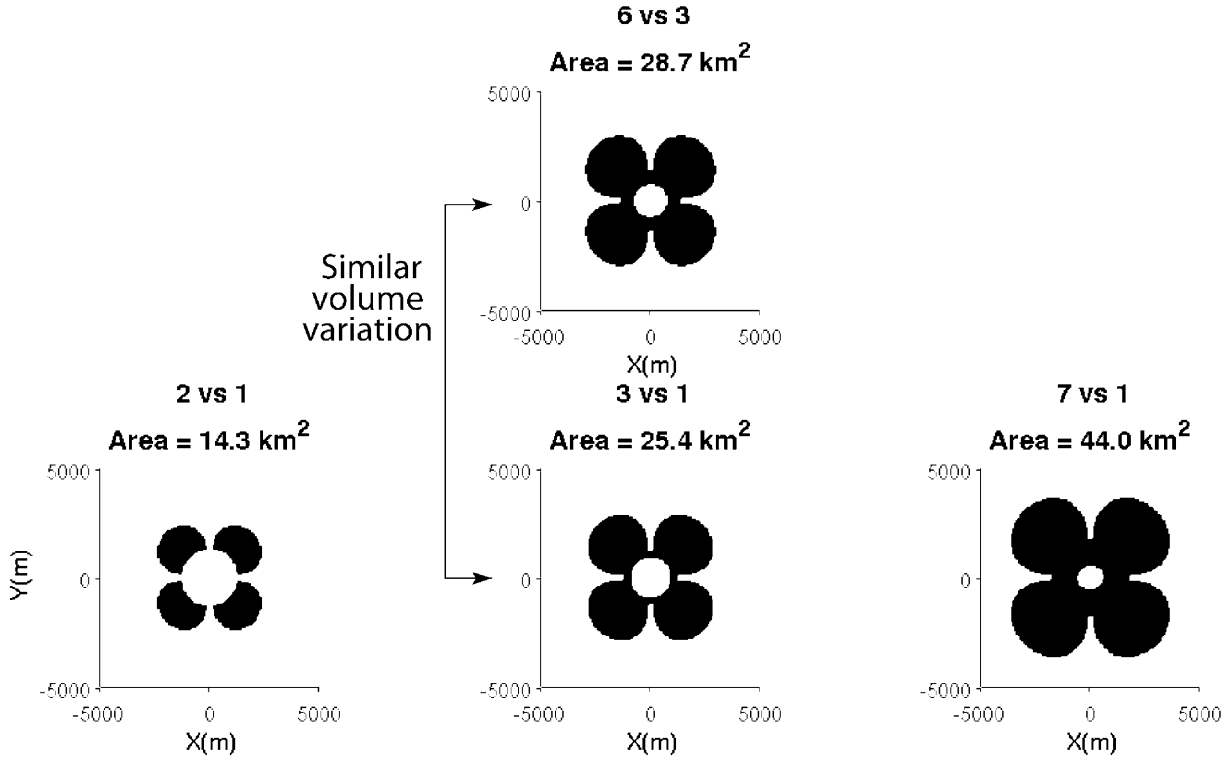



**Figure 7.** Measurable zone of the Ey component for a deep horizontal electric dipole (100 m, 10 A, 1 Hz). Conditions are as follows: Relative amplitude variations >1% and absolute amplitude variations >1 nV/m. The variations represented here are with respect to the initial state 1 of the reservoir. The graph showing the step from state 3 to state 6 has been added for the purposes of comparison with the step from state 1 to state 3, which corresponds to a similar volume of fluid substitution.

[26] Since low-frequency electromagnetic involves the diffusion equation, we can expect better information concerning the global volume and position of the fluid substitution, than concerning the geometric shape of the water front. The estimation of the volume of oil that can be produced is just as important as the distance of the water front from the production wells. For this reason, the behavior of the 4-D CSEM response, for the same volume of change, but for a different shape, will be observed in order to determine the sensitivity of the measurement device to the geometric shape of the WOC.

[27] All the profile plots presented in this paper correspond to the x axis, with the y coordinate being fixed at 0 m. The length of the electric dipole source is set to 100 m, and its intensity to 10 A.

### 3.1. Buried Horizontal Dipole

[28] Figure 4 shows the relative variation of the amplitude, in-phase and quadrature parts of the two orthogonal horizontal electric components Ex and Ey measured on the Earth's surface. The divergence of the horizontal components (Figure 4, right) is discussed later. The time-lapse signal corresponds to the difference measured between states 1 and 3 (see Table 1). The Ey component produces a weaker relative response than the Ex component, since the darker EM zones corresponding to high relative variations are less present. This is explained by the fact that the source is x-oriented. It is important to note that additional high relative variation zones (above 5%) can be identified with the in-phase and quadrature parts of the complex electromagnetic field. These zones are contained inside the 3 km radius, which is drawn on all surface plots. It is thus likely that relative variations inside these areas are significant. This outcome highlights the need to interpret the complex field rather than the amplitude data only.

[29] As mentioned before, the amplitude variation itself has to be checked in order to ensure that the 4-D signal amplitude remains above the assumed instrumental sensitivity of 1 nV/m for the electric field (100 nV for a 100 m long receiver). The measurable zones of both Ex and Ey components are considered to be those where both conditions, i.e., concerning the relative (>1%) and absolute variations (>1 nV/m), are verified. Figure 5 shows the measurable zone for the Ex component, by determining the time difference with respect to the initial state 1. The measurable zone has a comparatively large surface area, greater than 10 $km^2$, for a target at a depth of only 1 km. This measurable zone grows as long as the reservoir is pumped. Its size and shape are similar if we compare the 3vs1 and 6vs3 steps, which have the same volume variations but different shapes (Table 1).

[30] Figure 6 shows how the measurable zone changes when closer time monitoring is made. The comparison is not made with the initial state 1, but with the previous state (i-1). The measurable zone vanishes almost com-

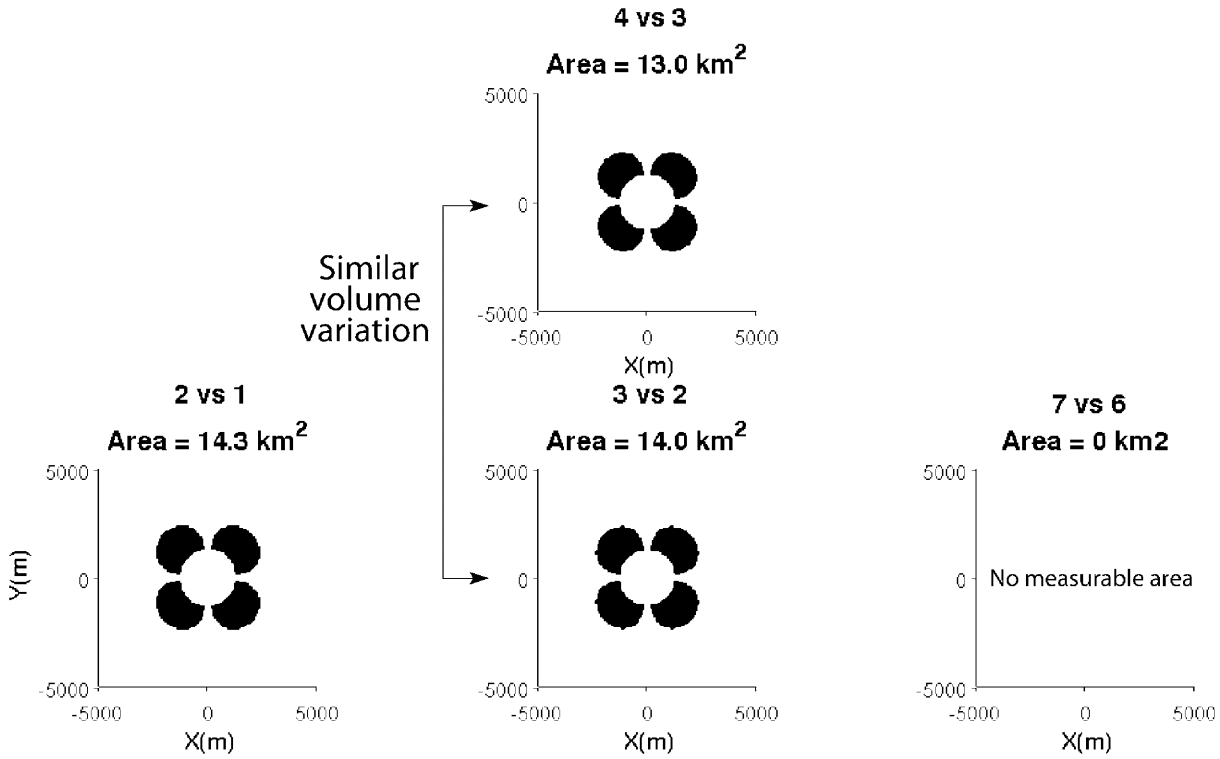



**Figure 8.** Measurable zone of the Ey component for a deep horizontal electric dipole (100 m, 10 A, 1 Hz). Conditions are as follows: Relative amplitude variations >1% and absolute amplitude variations >1 nV/m. The variations represented here are with respect to the previous state (i-1) of the reservoir. The graph showing the step from state 3 to state 4 has been added for the purposes of comparison with the step from state 2 to state 3, which corresponds to a similar volume of fluid substitution.

pletely when the last states of the reservoir are monitored. The same observations can be made for the Ey component in Figure 7, shown in comparison with the initial state 1, and in Figure 8, shown in comparison with the previous state (i-1). From the initial state, the measurable zone of Ey also has a significant surface area, greater than 10 km$^2$, despite the x-oriented electric dipole (Figure 7). The measurable zone also vanishes in the case of short time interval monitoring of the last reservoir states (Figure 8). As observed for the Ex component (Figures 5 and 6), the measurable area of Ey is similar if the volume of change is identical (Figures 7 and 8). This indicates that the device with a horizontal electric dipole source is more sensitive to changes in volume than to the geometric shape of the water front.

[31] Since the measurable zones of Ex and Ey intersect (see Figures 5 and 7), it is of interest to compute $\partial Ez/\partial z$ from these two horizontal components, according to equation (10) (Figure 4, right), which allows the relative variation (for the amplitude, in-phase and quadrature components) to be enhanced over a disc, having a geometry similar to that of the WOC movement.

### 3.2. Buried Vertical Dipole

[32] As for the horizontal dipole (Figure 4), Figure 9 shows the relative variation of the electromagnetic field measured at the Earth's surface, induced by a buried vertical electric dipole (still between states 1 and 3). If there is no zone for which the relative variation is largely above 5% at a maximum radial distance of 3 km from the source, the Ex and Ey receivers produce a relative amplitude response of approximately 4%, over a wide area. The quadrature components are seen to have a stronger relative response than the amplitude, over a large disc defined by inner and outer radii of approximately 1000 and 3500 m, respectively. Stronger relative variations can also be observed if the electromagnetic field is split into in-phase and quadrature components. Since the 3-D reservoir has vertical axis symmetry in each state, the relative variations of Ex and Ey are similar and axially symmetric. Both the x and y components should be retained in order to detect any asymmetric variation of the WOC.

[33] Figure 10 shows the measurable zone of the Ex component, considering the same thresholds as in Figure 5 (relative variation >1% and amplitude variation >1 nV/m), by making the time difference with respect to the initial state of the reservoir. The measurable zone is smaller than for a horizontal electric dipole (Figure 5), but is still quite large (more than 10 km$^2$). As can be seen (Figure 10), the surface area of the measurable zone is not the same for 6vs3 as for 3vs1, despite their identical volume variations. In numerical terms, it is 49% greater in the case of the 6vs3 step. This can be explained by the greater upper surface variation for the case of 6vs3 (1.56 km$^2$), when compared with 3vs1 (1 km$^2$),

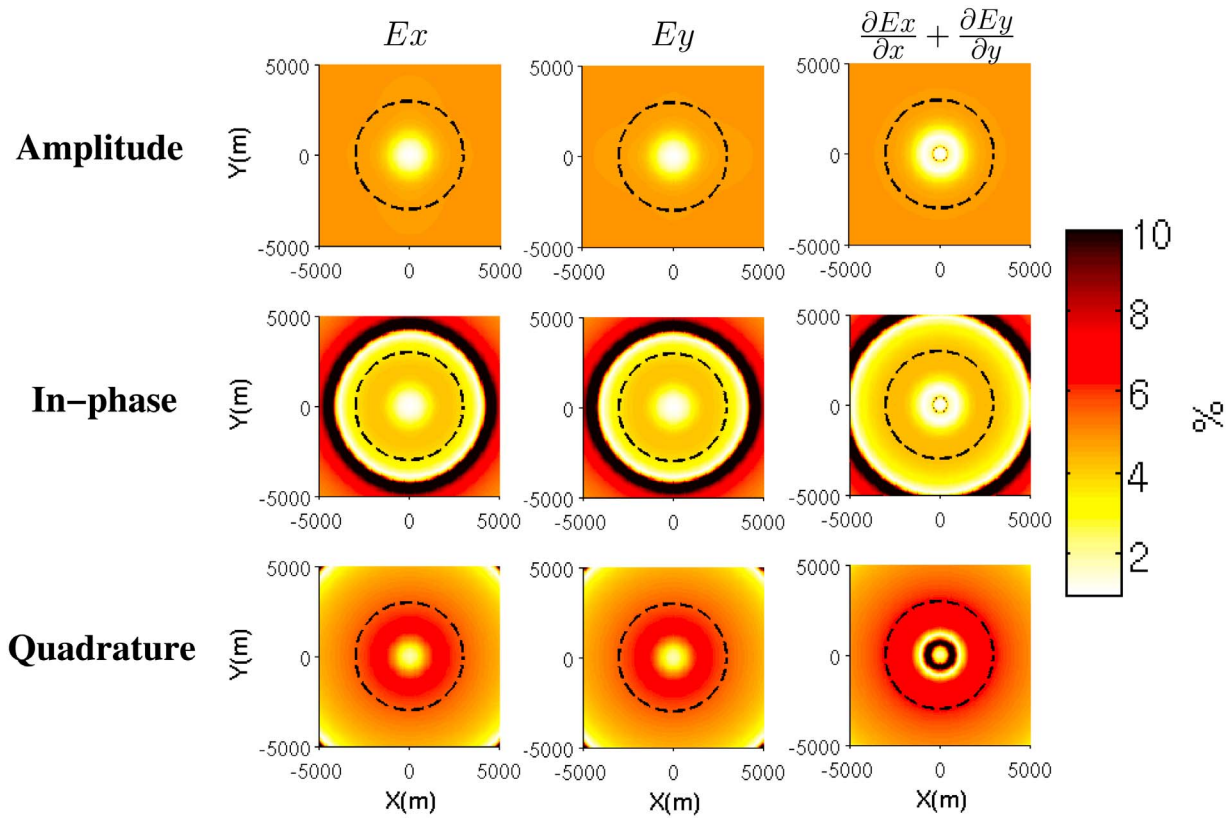



**Figure 9.** Relative variations (amplitude, in-phase, and quadrature components) for a deep vertical electric dipole (100 m, 10 A, 1 Hz), between states 1 and 3 of the reservoir (dashed line: circle of 3 km radius).

corresponding to a relative difference of 56%, as detailed in Table 1.

[34] Figure 11 shows the measurable zone, while comparing the consecutive states of the reservoir. The measurable area does not vanish during the monitoring of the last reservoir states, as it did in the case of the horizontal electric dipole (Figure 6). It remains greater than 10 km$^2$, and even increases slightly as the WOC get closer to the borehole, despite the decreasing variation in volume between the last states. In this case, when compared with the HED source, the VED source is less sensitive to the volume of replaced fluid. Nevertheless, the VED source allows lateral variations of the WOC to be monitored, even though the variations in volume are quite small, for example during the last states of the reservoir (see Table 1 for details). For the sake of simplicity, it was therefore decided to perform the sensitivity analysis using the buried vertical electric dipole source only.

[35] Since a vertical source is used, and it is assumed that the modeled reservoir has axially symmetric geometry, Ey and Ex can be expected to produce identical figures, with one rotated by 90 degrees with respect to the other. Since the measurable zones of the horizontal components are crossing, it is then interesting to compute $\partial Ez/\partial z$ from equation (10). Figure 9 (right) shows the relative variation of this derivative, when computed from the horizontal components. The amplitude and in-phase components do not exhibit strong relative variations above 5%, unlike those obtained for a horizontal electric dipole (see Figure 4, right). Only the quadrature component is characterized by a disc, where the relative variation is high, i.e., close to or greater than 10%. The computation of $\partial Ez/\partial z$ thus appears to be less beneficial in the case of a vertical dipole source than for a horizontal source. The phase and quadrature data again demonstrate their importance, since the strong relative variation is seen in the quadrature component only.

## 4. Influence of Background Resistivity Uncertainties on the 4-D Signal

[36] Errors due to uncertainties in the location of the source or the receiver are not discussed here, since the positioning problem does not really exist on land, when compared to the offshore case. However, a poor knowledge of the Earth's conductivity (i.e., background uncertainties) is definitely crucial, if prior fine-scale exploration has not been carried out, and/or has not been perfectly calibrated with well-log data.

[37] *Lien and Mannseth* [2008] have shown that uncertainties in the background Earth conductivity generally induce relative errors in the 4-D signal of the reservoir, which remain below 10% for the case of a 50% overestimation of the conductivity of a layer whose thickness is greater than 40 m. Here, we propose to consider, first, the effect of a missed, highly conductive (saline aquifer) thin layer, with a thickness of 10 m and a conductivity of 1 S/m, and, second, the effect of a very resistive (oil or gas

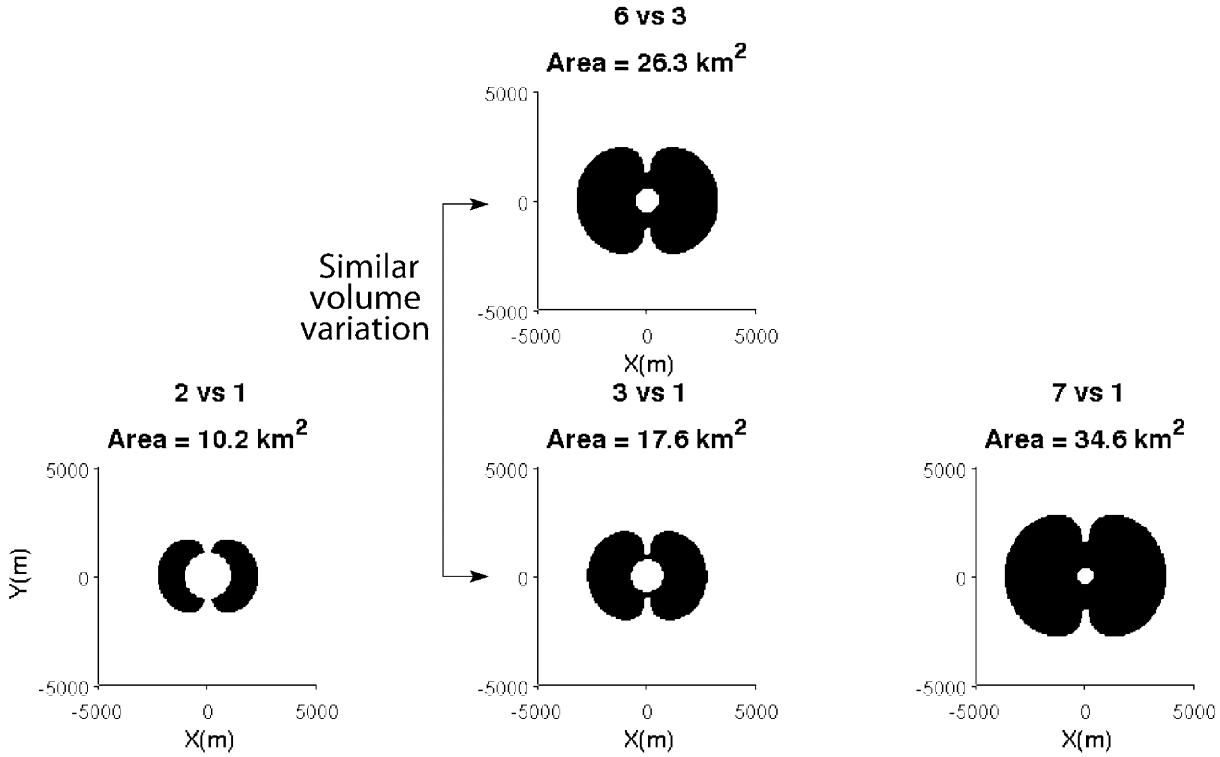



**Figure 10.** Measurable zone of the Ex component for a deep vertical electric dipole (100 m, 10 A). Conditions are as follows: Relative amplitude variations >1% and absolute amplitude variations >1 nV/m. The variations represented here are with respect to the initial state 1 of the reservoir. The graph showing the step from state 3 to state 6 has been added for the purposes of comparison with the step from state 1 to state 3, which corresponds to a similar volume of fluid substitution.

leakage) layer with a thickness of 10 m and a conductivity of 0.01 S/m. This layer will be located at different depths between the receivers and the top of the reservoir. Figure 12 provides a sketch of the different positions of this layer: N1 within the first 10 m below the surface; N2 at an intermediate distance between the source and the surface, or between the source and the reservoir; N3 in the vicinity of the dipole source; and N4 just above the oil-saturated part of the reservoir. Simulations of the N2 and N3 cases revealed only very small modifications to the time-lapse response of the reservoir, due to the presence of these thin layers, even when they are close to the dipole source. Moreover, the coupling effect between the reservoir and the thin layer will be maximum if the layer is located in the vicinity of the reservoir. For these reasons, only the N1 and N4 cases have been shown in this paper. The effects of these two 1-D heterogeneities have also been compared to those of 3-D bodies at the same locations.

[38] Two cases of 3-D near-reservoir heterogeneities were considered, both being located 100 m above the top of the reservoir, with the dimensions 500 m × 500 m × 100 m and 1500 m × 3000 m × 100 m, respectively. These were positioned in order to cover the water-oil contact during the reservoir's production (Figure 13). Since these 3-D bodies are close to the reservoir, they are included in the 3-D grid already generated for the oil reservoir, which allows only one 3-D heterogeneity to be considered, and are associated with the method of moments formalism. The effect of near-surface 3-D heterogeneities (500 m × 500 m × 100 m at a depth of 100 m, and 4000 m × 2000 m × 100 m at a depth of 200 m) were also studied. Their localizations were chosen so as to have the potentially greatest effect on the receivers for which the time-lapse signal is maximum (Figure 13). In order to model these additional heterogeneities using the method of moments, we applied the inhomogeneous background conductivity (IBC) method described by *Zhdanov et al.* [2006], which allows a 3-D background to be considered. In the case of near-surface bodies, the coupling effects with the deep 3-D reservoir are very small, such that with the IBC method, only a small number of alternative inductions between the two distant bodies is required, in order for the algorithm to converge.

### 4.1. Near-Reservoir Heterogeneity

[39] Near-reservoir heterogeneities are assumed to produce a greater disturbance to the coupling between cells used to discretize the reservoir with the method of moments (details in section 2), than heterogeneities located farther from the reservoir. The interactions between the cells of the reservoir are separated into two components: a primary component corresponding to the direct effect in a homogeneous medium, and a secondary component corresponding to the presence of layers which are different to the homogeneous medium.

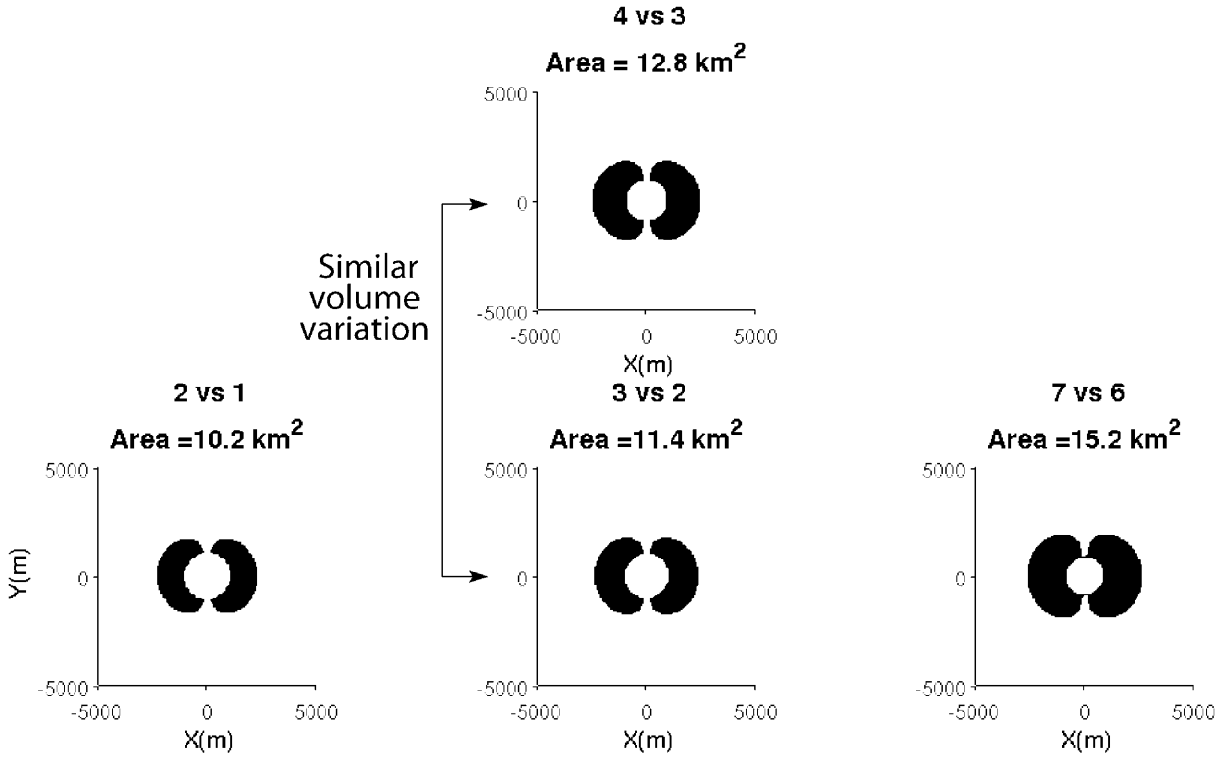



**Figure 11.** Measurable zone of the Ex component for a deep vertical electric dipole. Conditions are as follows: Relative amplitude variations >1% and absolute amplitude variations >1 nV/m. The variations represented here are with respect to the previous state (i-1) of the reservoir. The graph showing the step from state 3 to state 4 has been added for the purposes of comparison with the step from state 2 to state 3, which corresponds to a similar volume of fluid substitution.

[40] Figure 14 shows the relative variation in the 4-D amplitude of the Ex component, between states 1 and 3, along the x profile at $Y = 0$ m. Figure 14a shows the variation between the first states 1 and 3; the thin layer is located just above the top of the reservoir. The curves marked 1 S/m (conductive layer) or 0.01 S/m (resistive layer) correspond to the time-lapse signal between states 1 and 3, with the thin layer included in the background Earth which, as described

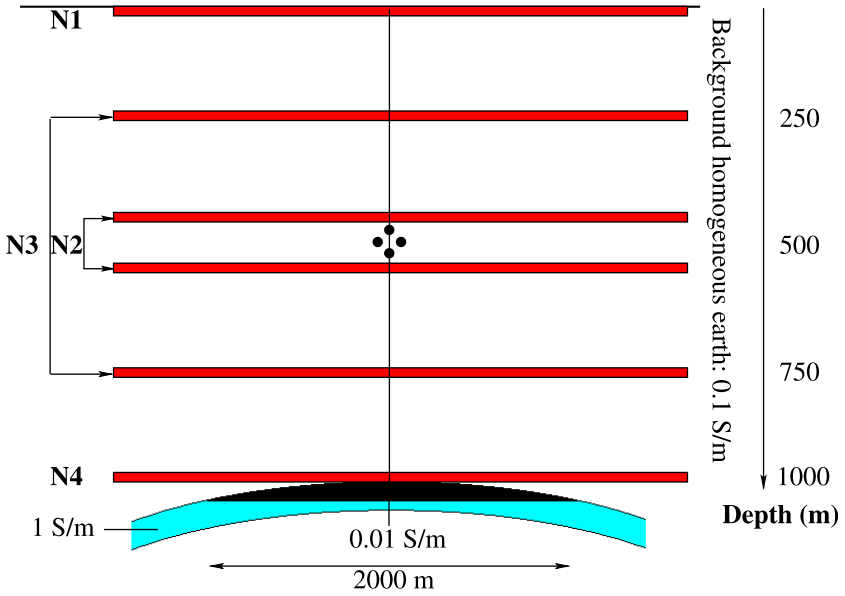



**Figure 12.** Synthetic case. Lack of knowledge of the background: 10 m conductive thin layer (1 S/m), or resistive thin layer (0.01 S/m) missed. N1, near surface; N2, near source; N3, intermediate distance; N4, near reservoir.

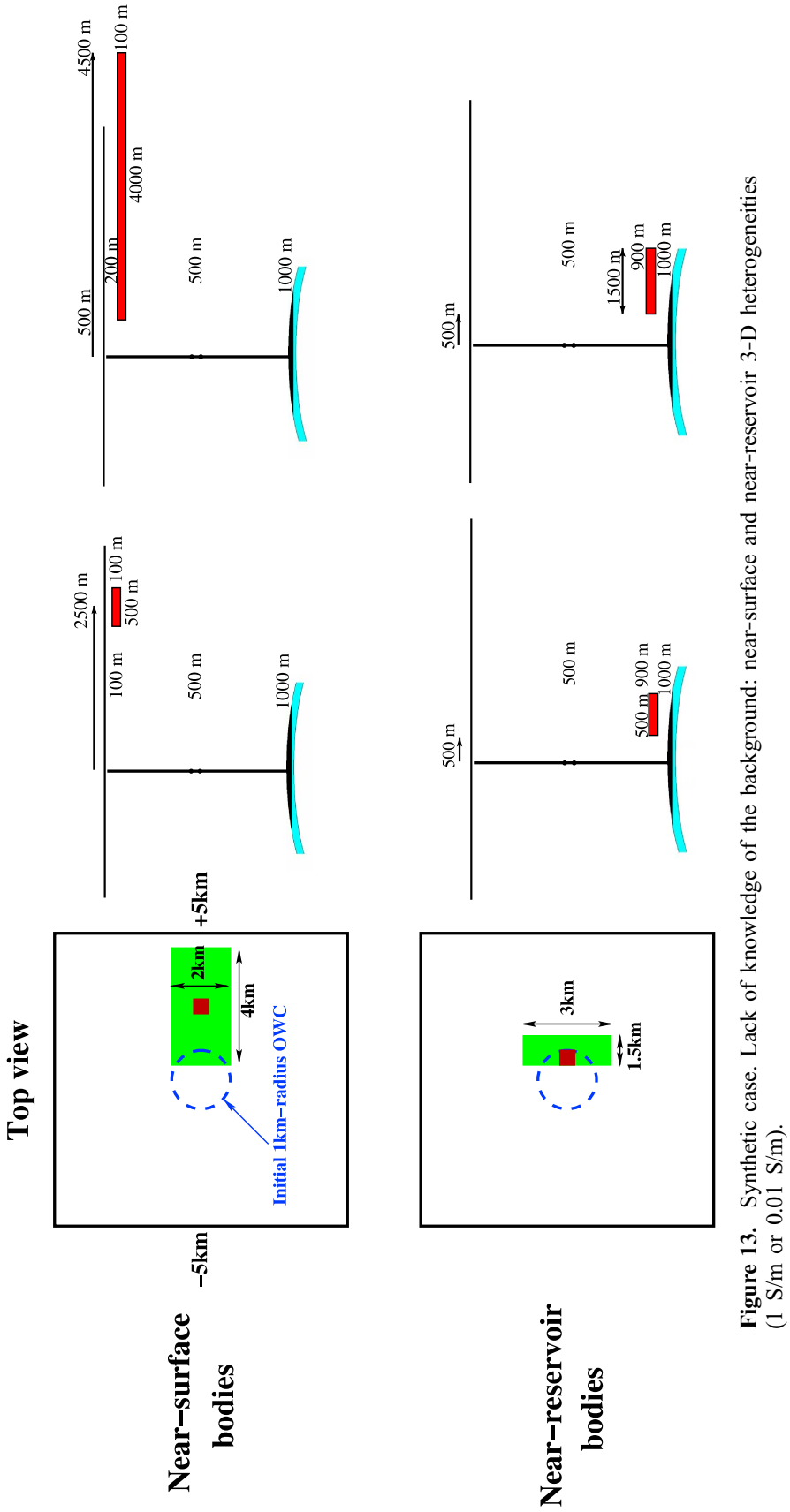



**Figure 13.** Synthetic case. Lack of knowledge of the background: near-surface and near-reservoir 3-D heterogeneities (1 S/m or 0.01 S/m).

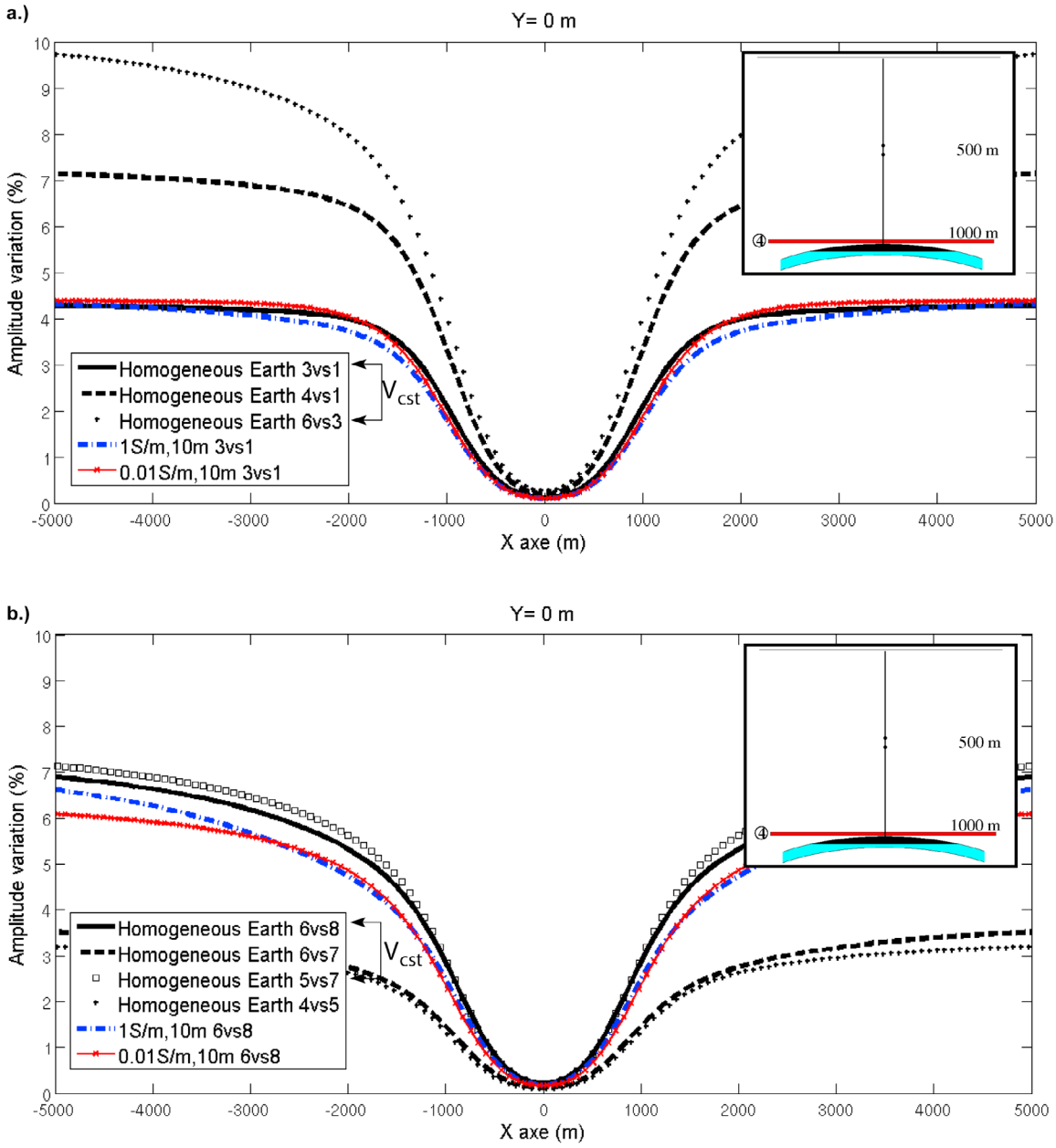



**Figure 14.** Effect of a near-reservoir thin layer on the relative amplitude variation of Ex, for a vertical electric dipole (100 m, 10 A, 1 Hz). Profile Y = 0 m. (a) Between states 1 and 3 of the reservoir. (b) Between the last states, 6 and 8, of the reservoir.

in section 3, was considered to be homogeneous. The other curves, 4vs1 and 6vs3, correspond to the time-lapse signal between states 1 and 4, and between states 3 and 6 (see Table 1 for details). The latter two curves are the responses with the initial, homogeneous Earth background (0.1 S/m). When the curves corresponding to the addition of the thin layer remain close to the 3vs1 curve and do not cross 4vs1 and 6vs3, this means that the effects of the thin layer have almost been canceled in the 4-D signal. This condition is observed for both conductive and resistive layers. Therefore, the effect of a very conductive (1 S/m), or very resistive (0.01 S/m), 10 m thick layer located just above the top of the reservoir (1000 m) will be almost completely damped in the 4-D signal, since the initial states of the reservoir are observed in this case.

[41] However, the change in the reservoir's cells between these two states occurs at a greater distance (40 m) from the thin layer than during the last states, for which the WOC is closer to the layer (<10 m). Figure 14b shows the 4-D relative signal between the last states, 6 and 8. The curves including the effect of the thin layer still do not cross the other monitoring curves associated with the homogeneous Earth: 5vs7, 6vs7, and 4vs5. Nevertheless, the gap between these curves and the homogeneous 6vs8

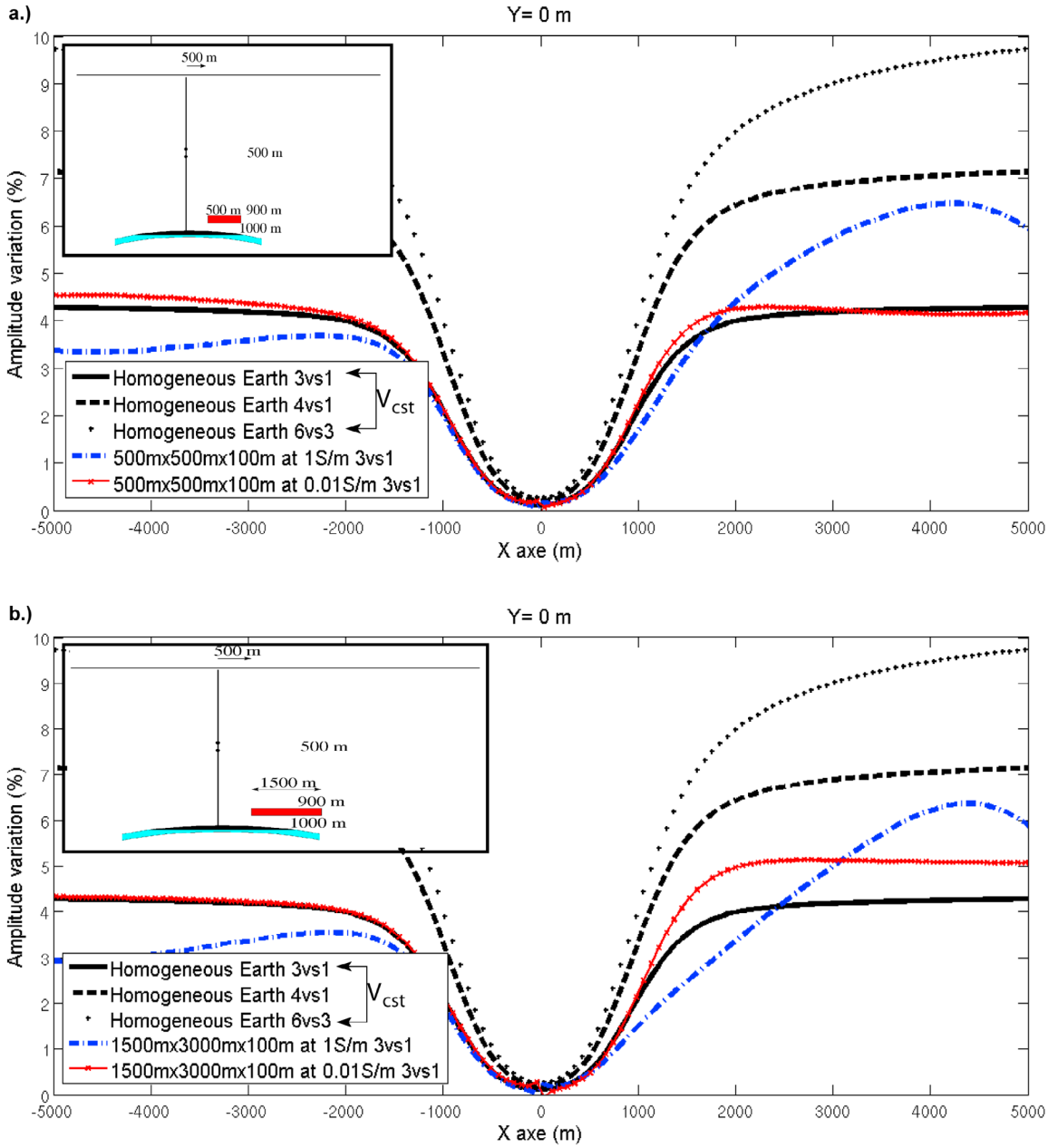



**Figure 15.** Effect of a near-reservoir 3-D body on the relative amplitude variation of Ex for a vertical electric dipole (100 m, 10 A, 1 Hz). Profile $Y = 0$ m. (a) Small, 500 m × 500 m × 100 m, 3-D body. (b) Large, 1500 m × 3000 m × 100 m, 3-D body.

curve is greater than that between the 3vs1 and conductive/resistive layer curves at the initial states of the reservoir (Figure 14a).

[42] A visible difference between the 6vs3 and 3vs1 curves, with similar volume variations, can be pointed out (Figure 14). This confirms that it is possible to separate the responses of two 4-D signals, if they are due to the same volume of fluid substitution, but to a different shape of water invasion. It can also be noticed that curves 4vs5 and 6vs8 are quite different (Figure 14b), despite similar quantities of fluid substitution. It is important to observe the proximity of the 5vs7 and 6vs8 curves. The volume of fluid replacement between states 5 and 7 (14.6 $Mm^3$) is greater than between 6 and 8 (9.8 $Mm^3$). This appears to compensate for the location of the fluid substitution which occurs at a further distance from the source borehole (from 700 to 500 m for 5vs7, and from 600 to 400 m for 6vs8). This outcome underlines the well known problem of equivalence, which can be encountered during data interpretation, especially during the inversion of time-lapse data.

[43] Figure 15 shows the 4-D relative variation in the amplitude of the Ex component, as in Figure 14a, but takes a 3-D heterogeneity into consideration, rather than an additional 1-D layer. Two different sizes of 3-D body

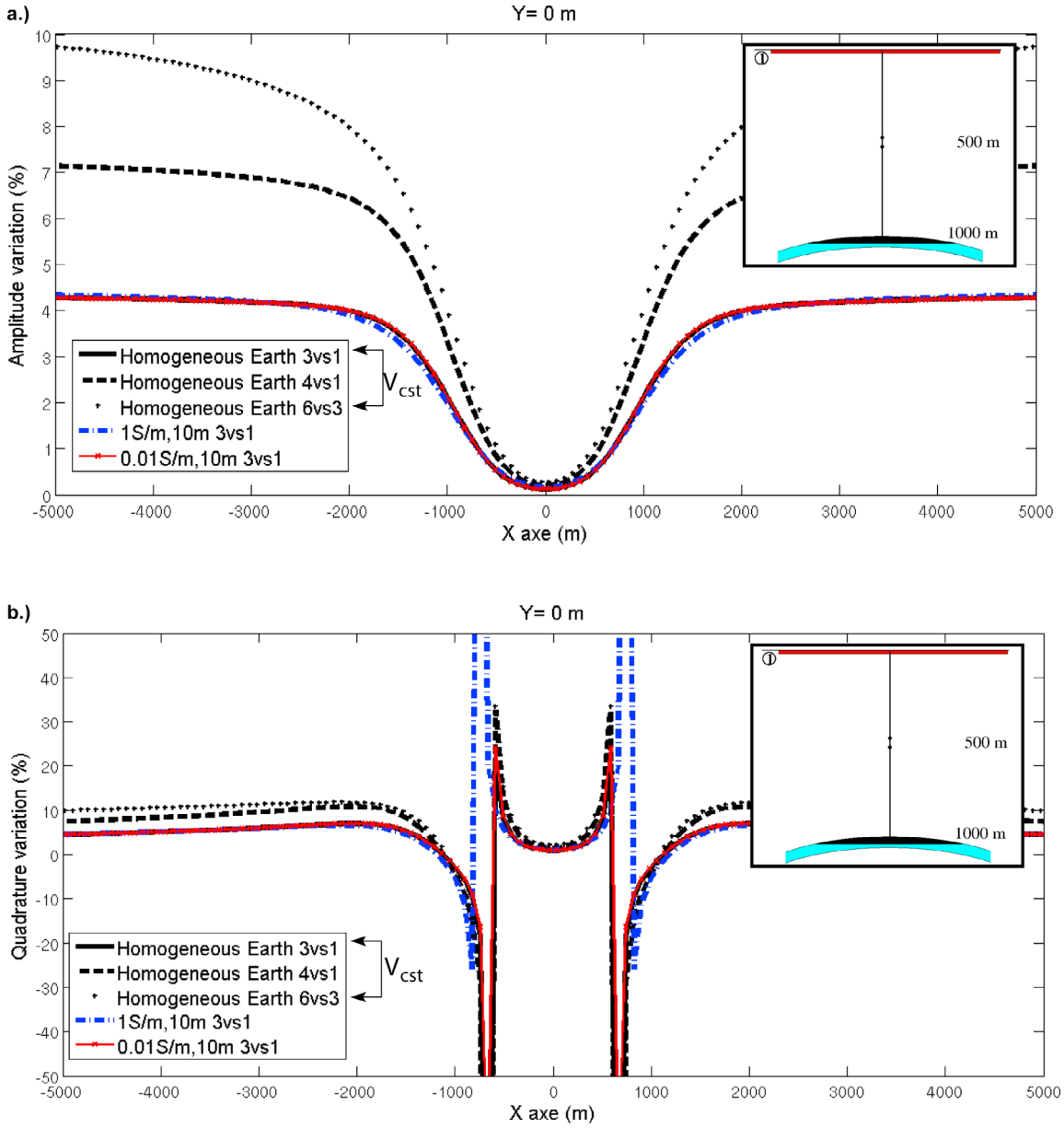



**Figure 16.** Effect of a near-surface thin layer on the relative amplitude variation for a vertical electric dipole (100 m, 10 A, 1 Hz). Profile $Y = 0$ m. (a) On Ex component. (b) On $\partial Ez/\partial z$ computed from Ex and Ey (equation (10)).

were considered: in Figure 15a, the body is relatively small (500 m × 500 m × 100 m), whereas in Figure 15b the body is larger (1500 m × 3000 m × 100 m). For both bodies, the nearest corner of the source borehole is located 500 m from the very top of the reservoir, in order to cover the WOC during production. Both types of heterogeneity are considered, i.e., more resistive and more conductive than the background.

[44] For the small, resistive 3-D body (Figure 15a), the curve remains close to the one for which a homogeneous Earth only was considered for the background. The shift due to the larger resistive 3-D body is more significant (Figure 15b), especially on the right side of the profile where the heterogeneity is located. Nevertheless, the curves are very close, for distances below 1.5 km from the source borehole. The left side is almost identical to the curve corresponding to a homogeneous background.

[45] The disturbance is substantially stronger when the 3-D body is considered to be conductive. For the smallest body (Figure 15a), the perturbation still allows the different curves to be separated at offsets below 2.5 km. However, the interpretation becomes more difficult when the conductive body is larger (Figure 15b), especially on the surface, immediately above the buried 3-D body.

[46] Fortunately, the presence of a resistive body due to a gas leakage above the oil-saturated part of the reservoir is

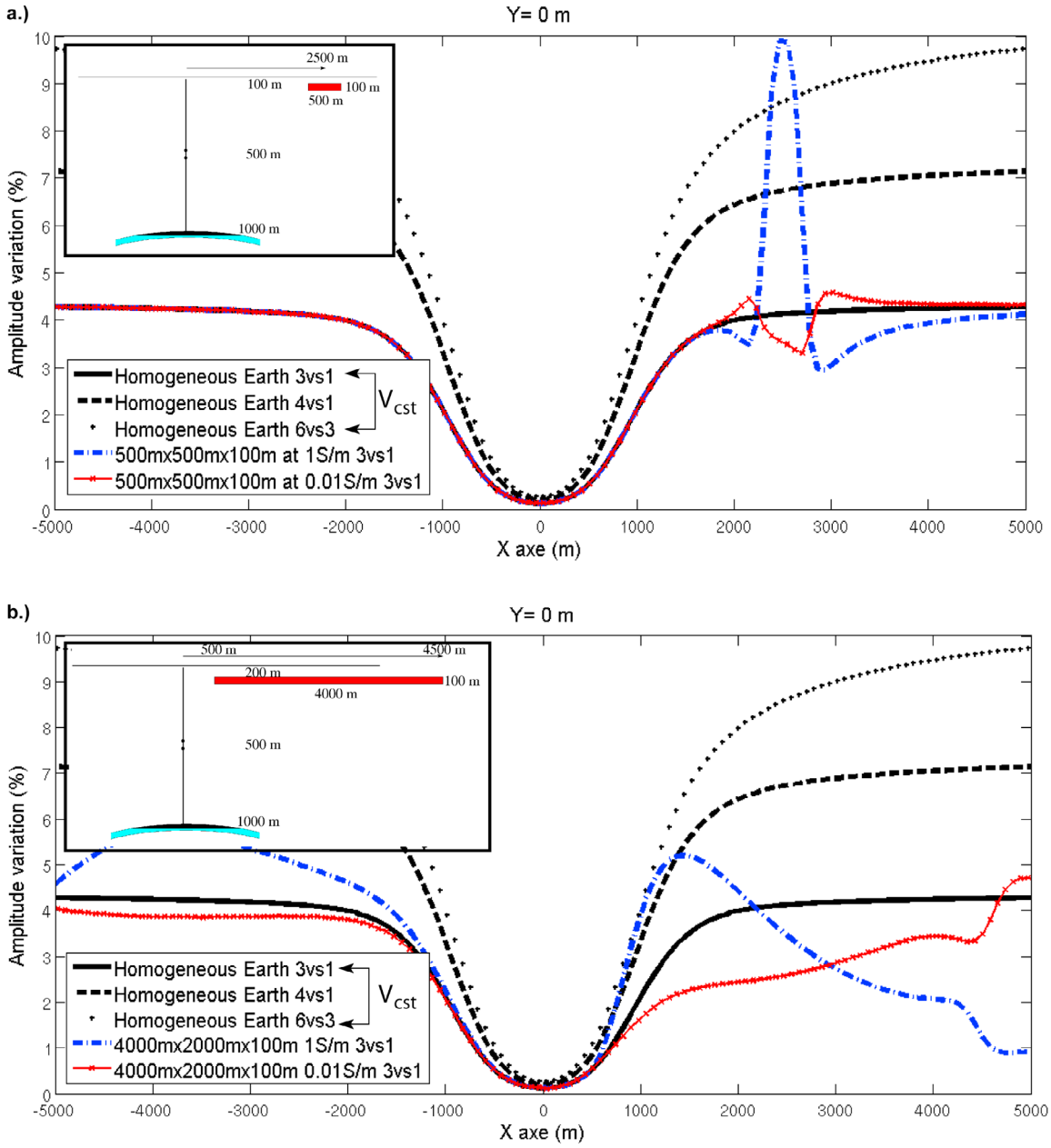



**Figure 17.** Effect of a near-surface 3-D body on the relative amplitude variation of Ex for a vertical electric dipole (100 m, 10 A, 1 Hz). Profile $Y = 0$ m. (a) Small, 500 m × 500 m × 100 m, 3-D body. (b) Large, 1500 m × 1500 m × 100 m, 3-D body.

more likely than the presence of a conductive body, which could occur in the case of a highly saturated water zone or a clay lens.

### 4.2. Near-Surface Heterogeneity

#### 4.2.1. No Time Variation

[47] Figure 16a is configured similarly to Figure 14a, with the exception that the thin layer is located in the first 10 m below the ground surface. The curves with the additional thin layer remain close to the 3vs1 curve. Therefore, a poorly described near-surface conductivity, which is stable in time, will not disturb the 4-D CSEM signal of the reservoir.

[48] Figure 16b shows the 4-D relative signal (based on $\partial Ez/\partial z$, determined using equation (10)), for the same setup as the one defined for Figure 16a. In accordance with Figure 9 (right), we chose to plot the relative variation of the quadrature component, since the dark disc corresponding to high relative variations is only visible in Figure 16b. The curve corresponding to the additional conductive layer is quite different to the 3vs1 curve, whereas the curve with the additional resistive layer remains very similar to the 3vs1 curve. The curve with a conductive layer also crosses the 4vs1 and 6vs3 curves. The influence of the thin conductive layer on the time-lapse signal is greater at shorter offsets, and tends to vanish as the offset grows (the curve with an

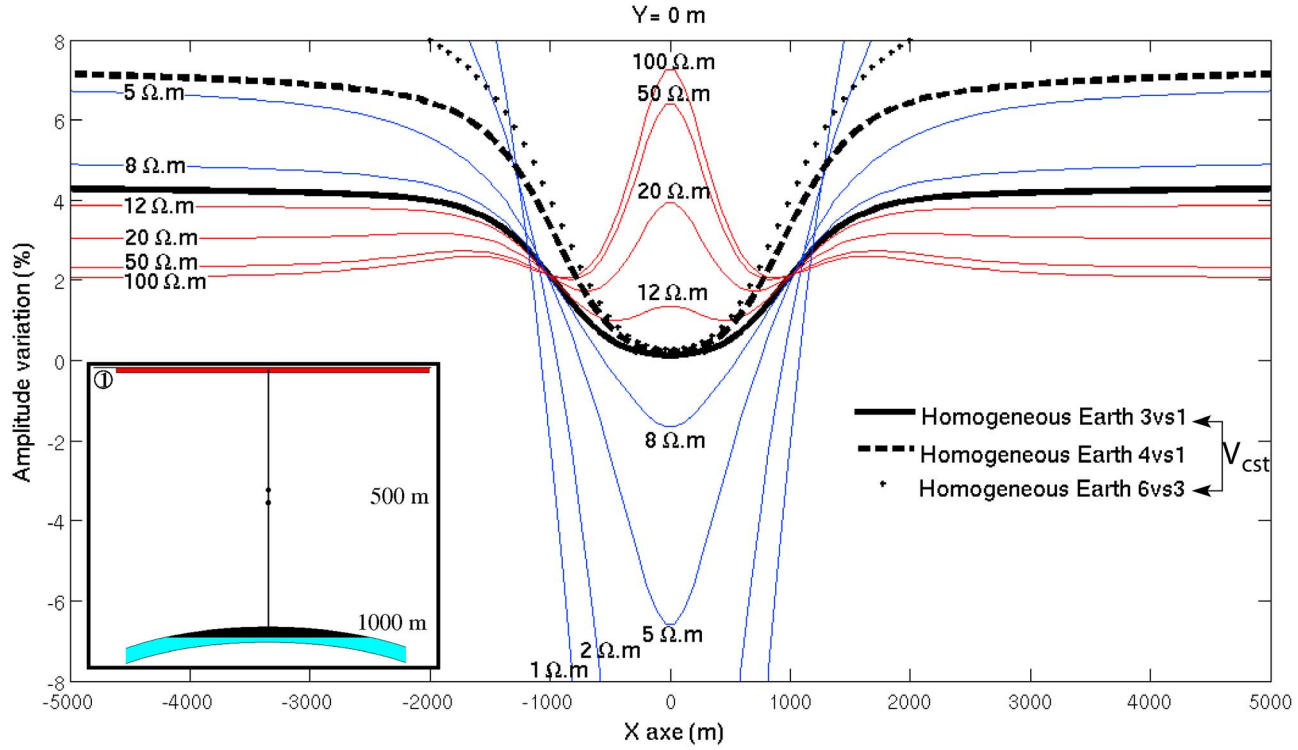



**Figure 18.** Effect of a change in near-surface conductivity, on the relative amplitude variation of the 4-D signal of the reservoir between states 1 and 3, for different changes in conductivity in the first 10 m (initially at 10 Ω m to 0.1 S/m). Profile of Ex component at $Y = 0$ m. Vertical electric dipole (100 m, 10 A, 1 Hz). The conductivity changes range from 0.01 to 1 S/m.

additional thin conductive layer approaches that of the 3vs1 curve). The perturbation due to the presence of the thin conductive layer occurs at distances from the borehole which are identified above (section 3.1) as leading to optimal offsets for the 4-D signal (see Figure 16b, between 500 and 1000 m). This strong effect can be explained by the fact that the Ez component is sensitive to a thin layer, such as a thin reservoir. Thus, in order to correctly interpret the time-lapse signal with such data transformations, the accurate determination of the location of a potentially conductive thin layer is mandatory.

[49] As in the case of Figure 15 for near-reservoir bodies, Figure 17 shows the impact of a near surface 3-D body, whose dimensions are similar to the examples given by *Sasaki and Meju* [2009]: in Figure 17a, the body is relatively small (500 m × 500 m × 100 m) and located at a depth of 100 m, whereas in Figure 17b the body is larger (4000 m × 2000 m × 100 m), and located at a depth of 200 m. These 3-D bodies are positioned so as to be close to the receivers, where the 4-D CSEM signals from the reservoir production produce an optimal response.

[50] For the small 3-D body (Figure 17a), the perturbation is focused on the area just above the near-surface heterogeneity. The rest of the curve remains unchanged, and the modified part could even be filtered to remove the peak perturbation response of this body.

[51] For the large 3-D body (Figure 17b), the effect on the 4-D reservoir signal is very strong on the right side, where the heterogeneity is located, for both resistive and conductive bodies. On the left, the influence of the resistive body is not strongly penalizing and still authorizes valid interpretation of the time-lapse signal. The impact of the conductive body remains strong on this side, for offsets greater than 1.5 km. Figure 17b shows that ignoring the presence a large 3-D body located near to the surface could seriously damage the interpretation of the time-lapse signal emerging from the production of the reservoir. However, such vast heterogeneities (thickness of 100 m), should clearly be detected during the exploration campaign. Although the precision with which the boundaries of these 3-D bodies can be determined remains problematic, the resulting lack of accuracy can be considered to be similar to the very local influence of small 3-D heterogeneities on the receiver array, as can be seen in Figure 17a.

#### 4.2.2. Time Variation

[52] Near-surface conductivities are subjected to non negligible variations on land, because of varying weather conditions, especially rainfall variations. The 4-D signals resulting from near-surface conductivity changes (first 10 m) thus overlap with the time-lapse signature of the reservoir.

[53] Figure 18 shows the superposition of the 4-D reservoir signal with the time-lapse response of different near-surface conductivity changes, ranging from 0.01 to 1 S/m. The curves marked with a resistivity contain both the 4-D signal of the 3vs1 step of the reservoir, and the 4-D response due to the change in resistivity, in the first 10 m below the Earth's surface.

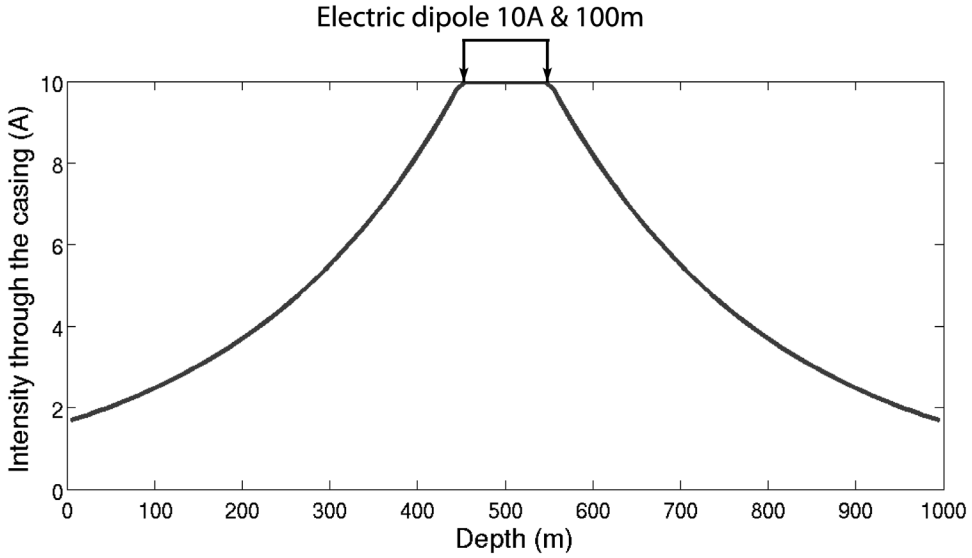



**Figure 19.** Electric current distribution inside a steel casing ($\sigma = 10^6$ S/m) surrounding the source borehole (from equation (11)).

[54] The thick solid line corresponds to the time-lapse signal between states 1 and 3, assuming the Earth to remain homogeneous. Curves 4vs1 and 6vs3 were added in order to determine whether the curves, which also contain the time-lapse response of the near-surface, cross these two 4-D signals; this would mean that the 3vs1 4-D signal is sufficiently perturbed by the time-lapse signal of the near-surface conductivity change, to be misidentified with other reservoir monitoring signals.

[55] The shapes of the curves are quite different at short offsets from the source borehole (below 1000 m), when the near-surface conductivity changes. Moreover, the curves for which there are deep reservoir changes only are grouped around 0% and are not distinguishable despite the different steps of the reservoir production. The 4-D reservoir signal is negligible inside this interval (below 1000 m). It is thus possible to directly detect potential near-surface effects, using receivers placed near to the source borehole, since the time-lapse signal for deep reservoirs is nonexistent at such short distances.

[56] Beyond a distance of 1 km from the borehole (source location), the curve closely approaches the 4vs1 step when the resistivity decreases to 5 Ω m (100% increase in conductivity). The curve corresponding to an increase in resistivity, up to 50 Ω m (80% decrease in conductivity), is located at the same distance from 3vs1 as the curve corresponding to a decrease to 5 Ω m. In the extreme case where the near surface becomes highly conductive (changing from 0.1 to 1 S/m), the 4-D signal resulting from an increase in conductivity in the first 10 m completely overwhelms the 4-D signal resulting from changes in the deep reservoir (1000 m).

## 5. Steel Cased Borehole

### 5.1. At the Source Location

[57] Old production and monitoring boreholes are often cased with metallic alloys, generally steel, which are a serious obstacle during cross-well EM tomography or diagraphy, especially when the frequencies used are greater than a few hundred hertz. At a few hertz, the problem of a steel cased borehole is not thoroughly established, as a consequence of the skin depth, which is approximately ten times the usual thickness of the steel casing. In fact, by considering a conductivity in the range $10^6$ to $10^7$ S/m and a relative magnetic permeability equal to 100, the skin depth is approximately 20 cm, which is about 10 times the classical casing thickness. Following the work of *Kaufman* [1990] developed for the DC case, *Kong et al.* [2009] have recently proposed an original study of casing effects in sea-to-borehole CSEM, in which the source and the steel cased borehole are replaced by a long antenna (a dipole series with an exponentially decreasing intensity). *Kong et al.* [2009] have shown that at 1 Hz, and with the above mentioned steel properties, the DC approximation of *Kaufman* [1990], which is a straightforward equivalence formulation, can be used to replace the source located in a steel casing by a large dipole antenna (equation (11) and Figure 19):

$$I(z) = I_0 \exp\left(-z\sqrt{\frac{\sigma_f}{S_c}}\right)$$
$$S_c = \sigma_c \times 2\pi r_i (r_o - r_i) \tag{11}$$

where

$I(z)$ current intensity (A) along the casing at a distance $z$ from the electric dipole (m),
$\sigma_f$ conductivity of the formation surrounding the casing (S/m),
$\sigma_c$ conductivity of the casing (S/m),
$r_i$ inner radius of the casing (m),
$r_o$ outer radius of the casing (m).

The example shown in Figure 20 shows the impact of replacing a steel casing by an equivalent dipole distribution (equation (11) and Figure 19). The time-lapse signal, although less pronounced than the results without a casing (<4%), is close to the casing-less curve below 1.5 km, and

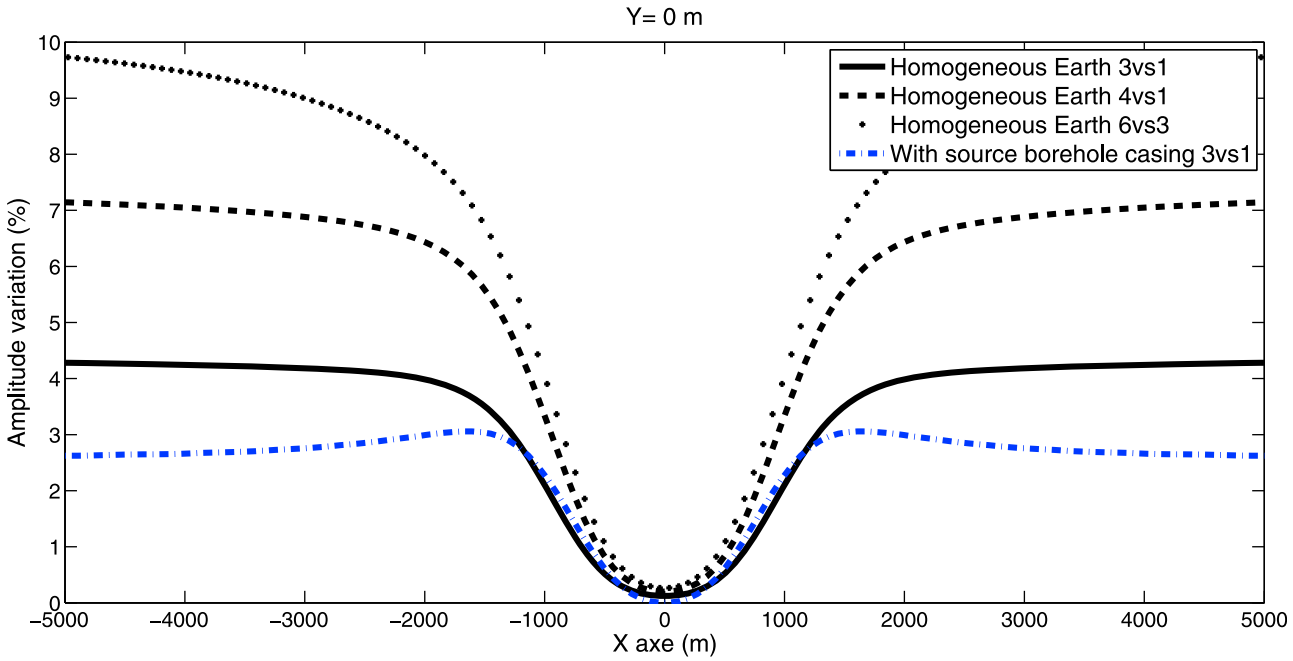



**Figure 20.** Effect of a steel casing, surrounding the source borehole, on the relative amplitude variation of Ex for a vertical electric dipole (100 m, 10 A, 1 Hz). Profile $Y = 0$ m. Between states 1 and 3 of the reservoir.

is still stronger than 1% for distances from the source borehole between 1 km and 1.5 km.

### 5.2. Outlying Cased Borehole

[58] For the case of an outlying cased borehole, it was decided to model the casing as a solid cylinder, with a volume equivalent to a hollow cylinder with an outer diameter of 20 cm, and an inner diameter of 18 cm. To model this additional heterogeneity using the method of moments, we used the previously described IBC method applied to the former rectangular 3-D bodies [*Zhdanov et al.*, 2006]. The effect of the outlying steel casing (located

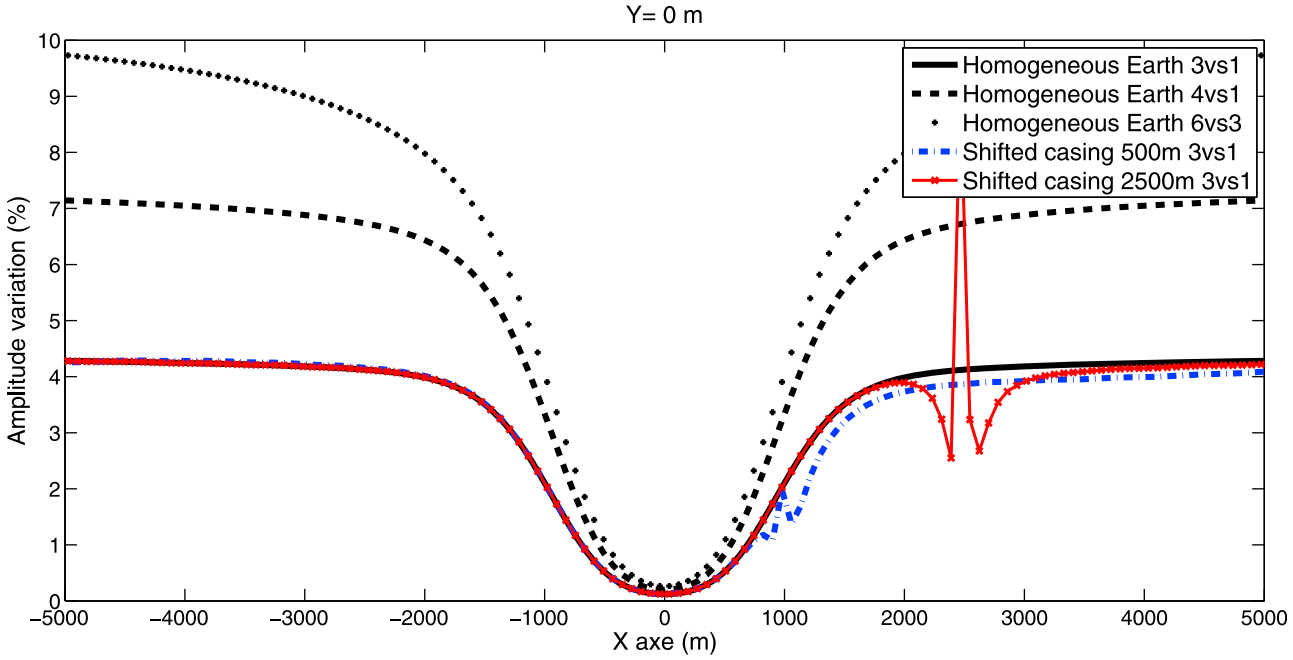



**Figure 21.** Effect of a steel casing offset (by 1000 or 2500 m from the source borehole) on the relative amplitude variation of Ex, for a vertical electric dipole (100 m, 10 A, 1 Hz). Profile $Y = 0$ m. Between states 1 and 3 of the reservoir.

at 2500 m from the source), shown in Figure 21, indicates a very localized signature with a maximum amplitude very similar to that which was recorded in the case of the 3-D near-surface conductive body of 500 m × 500 m × 100 m (Figure 17a). At a shorter distance (1 km), the effect is more pronounced (Figure 21) but still permits reliable interpretation. Clearly, the effect of a nearby, outlying cased borehole (i.e., located at a distance smaller than the depth of the reservoir) is sufficiently significant and disturbing to generate a nontrivial effect on the interpretation of the time-lapse signal.

## 6. Conclusion

[59] Several issues have been highlighted, concerning the land-based monitoring of WOC, in particular the use of a VED or HED electric source, the distribution of surface receivers, the system's sensitivity at large offsets, the influence of resistive or conductive 1-D layers or 3-D anomalies, near-surface time varying properties, and the influence of a centered or outlying steel casing. In order to simplify the presentation of this parametric study, the reservoir model and its temporal evolution used for all of the tests is axisymmetric, and the source dipole, either vertical or horizontal, has its center located on the axis of revolution. It is important to notice that only the frequency of 1 Hz has been used and that a dense grid of HED receivers was used (receiver spacing of the order of one tenth of the reservoir depth). Our key results are summarized below:

[60] 1. Among the different setups studied with a buried source and surface receivers, the use of a vertical electric dipole source is more sensitive for the monitoring of the last states of the reservoir, for which a horizontal electric dipole source delivers a weak 4-D signal. In the case of a HED source, the electric field measured at the surface is related essentially to the volume variation of oil-filled rocks (which becomes smaller during the final states of the reservoir evolution), whereas a VED source is shown to be highly sensitive to the shape of the fluid substitution. Since the time-lapse signal response can be very different, even when the changes in volume are identical, the VED source is preferred in the present study.

[61] 2. Analysis of the time-lapse signal reveals the need to treat complex data, which certainly contains complementary information, in addition to the amplitude. The evaluation of $\partial Ez/\partial z$ (based on equation (10)) allows the measurement system's sensitivity to lateral variations in the thin reservoir to be improved. However, it is also very sensitive to the eventual presence of an unresolved thin layer associated with the background, which could lead to uncertainties in the interpretation of the data.

[62] 3. In general, it was observed that the presence of an additional thin tabular layer, having a strong resistive or conductive contrast with the surrounding rocks, induces a small perturbation to the time-lapse signal of the reservoir, except when the layer is close to the reservoir. Near-surface 3-D anomalies clearly have a more significant effect than near-reservoir 3-D anomalies, because of their proximity to the receivers. However, small near-surface 3-D anomalies, with a lateral extent smaller than a few hundred meters, or bad definition of the extent of large 3-D bodies, have a localized perturbation.

[63] 4. The natural variation of the near-surface conductivity change can be significant, with an increase or decrease of 80% with respect to the initial state value. The results obtained in such a case revealed a strong modification of the time-lapse signal, which indicates the need to carefully follow near-surface resistivity changes during monitoring, by means of more or less local CSEM or electrical exploration methods.

[64] 5. The steel casing effect has been quantified for both centered (i.e., at the source location) and outlying positions. Considering the difficulties inherent to the extreme discretization of the cylinder thickness and the reservoir geometry, the equivalent dipole formalism provided by *Kaufman* [1990] appears to be an elegant and efficient technique for studying an energized casing. Preliminary results have shown no significant influence on the time-lapse signal, when the source borehole is cased. For an outlying steel casing, the method of moments allows an equivalent solid cylinder to be implemented; in such a configuration, the 4-D signal is significantly perturbed when the casing is placed at a distance equal to or smaller than the depth of the reservoir. Otherwise, a strong, but local perturbation is visible on the time-lapse signal.

[65] In conclusion, this theoretical study, based on a schematic but representative reservoir model of on-land monitoring of the WOC, has shown that this MoM code offers flexible and robust forward modeling, as required by future inversion schemes. Despite the computational cost of an increasing number of 3-D anomalies, the present MoM code can be considered as a technique, which is complementary to full domain discretization methods such as finite difference frequency domain (FDFD) or finite element method (FEM).

[66] **Acknowledgments.** This study makes use of results produced by the Enabling Grids for E-sciencE project, a project cofunded by the European Commission (under contract INFSO-RI-031688), in the context of the Sixth Framework Programme. EGEE brings together 91 partners in 32 countries to provide a seamless grid infrastructure available to the European research community 24 h a day. Full information is available at http://www.eu-egee.org. The authors wish to thank the reviewers for their professional and constructive comments, which have allowed them to improve this paper, as well as the Associate Editor M. A. Meju for his numerous suggestions. The authors extend their thanks to those who provided assistance in the crosschecking of the simulation code and fruitful discussions: M. Wirianto and W. Mulder from TU-Delft university and S. Baakr, T. Mannseth, and M. Lien from CIPR in Bergen University. Particular thanks are extended to G. Vetois and J. B. Favreau from CGGVeritas for their very useful technical support. We also wish to thank the CCR (Centre de Calcul et de Recherche) of the University of Pierre et Marie Curie for providing access to their JS21 and JS22 IBM machines. Special thanks to M. Krawczyk for his assistance.

## References

Andréis, D. (2008), Electromagnetic surveying for resistive or conductive bodies, U.S patent 7362102, U.S. Patent Off., Alexandria, Va.

Andréis, D., and L. MacGregor (2008), Controlled-source electromagnetic sounding in shallow water: Principles and applications, *Geophysics*, *73*(1), F21–F32.

Augustin, A. M., W. D. Kennedy, H. F. Morrison, and K. H. Lee (1989), A theoretical study of surface-to-borehole electromagnetic logging in cased holes, *Geophysics*, *54*(1), 90–99, doi:10.1190/1.1442581.

Barrowes, B. E., F. L. Teixeira, and J. A. Kong (2001), Fast algorithm for matrix-vector multiply of asymmetric multilevel block-Toeplitz matrices in 3-D scattering, *Microwave Opt. Technol. Lett.*, *31*(1), 28–32.

Cadoret, T., D. Marion, and B. Zinszner (1995), Influence of frequency and fluid distribution on elastic wave velocities in partially saturated limestones, *J. Geophys. Res.*, *100*(B6), 9789–9803.

Eidesmo, T., S. Ellingsrud, L. M. MacGregor, S. Constable, M. C. Sinha, S. Johansen, F. N. Kong, and H. Westerdahl (2002), Sea bed logging (SBL), a new method for remote and direct identification of hydrocarbon filled layers in deepwater areas, *First Break*, *20*, 144–152.

Guptasarma, D., and B. Singh (1997), New digital linear filters for Hankel $J_0$ and $J_1$ transforms, *Geophysical prospecting*, *45*(5), 745–762.

He, Z., X. Liu, W. Qiu, and H. Zhou (2005), Mapping reservoir boundary by borehole-surface TFEM: Two case studies, *Leading Edge*, *24*, 896–900, doi:10.1190/1.2056379.

Hohmann, G. W. (1975), Three-dimensional induced polarization and electromagnetic modeling, *Geophysics*, *40*(2), 309–324.

Hördt, A., P. Andrieux, F. M. Neubauer, H. Rüter, and K. Vozoff (2000), A first attempt at monitoring underground gas storage by means of time-lapse multichannel transient electromagnetics, *Geophys. Prospect.*, *48*(3), 489–509.

Kaufman, A. A. (1990), The electrical field in a borehole with a casing, *Geophysics*, *55*(1), 29–38, doi:10.1190/1.1442769.

Kong, F. N., F. Roth, P. A. Olsen, and S. O. Stalheim (2009), Casing effects in the sea-to-borehole electromagnetic method, *Geophysics*, *74*(5), F77–F87, doi:10.1190/1.3173807.

Lien, M., and T. Mannseth (2008), Sensitivity study of marine CSEM data for reservoir production monitoring, *Geophysics*, *73*(4), F151, doi:10.1190/1.2938512.

Liu, H., Z. Wang, and Z. He (2008), Frequency-domain 3-D borehole-surface electromagnetic modeling by the volume integral equation method, paper presented at 70th EAGE Conference and Exhibition, Eur. Assoc. of Geosci. and Eng., Rome.

Newman, G. A. (1994), A study of downhole electromagnetic sources for mapping enhanced oil recovery processes, *Geophysics*, *59*(4), 534–545, doi:10.1190/1.1443614.

Oehler, D., and B. Sternberg (1984), Seepage-induced anomalies, "false" anomalies, and implications for electrical prospecting, *AAPG Bull.*, *68*(9), 1121–1145, doi:10.1190/1.1442769.

Orange, A., K. Key, and S. Constable (2009), The feasibility of reservoir monitoring using time-lapse marine CSEM, *Geophysics*, *74*(2), F21–F29, doi:10.1190/1.3059600.

Pellerin, L., and G. Hohmann (1995), A parametric study of the vertical electric source, *Geophysics*, *60*(1), 43–52, doi:10.1190/1.1443761.

Sasaki, Y., and M. A. Meju (2009), Useful characteristics of shallow and deep marine CSEM responses inferred from 3-D finite-difference modeling, *Geophysics*, *74*(5), F67–F76, doi:10.1190/1.3168616.

Schamper, C. (2009), Study by simulations of the monitoring of reservoir production by electromagnetic methods., Ph.D. thesis, Univ. of Pierre and Marie Curie, Paris.

Schamper, C., S. Spitz, and A. Tabbagh (2008), Feasibility of EM monitoring in land reservoirs, paper presented at 70th EAGE Conference and Exhibition, Eur. Assoc. of Geosci. and Eng., Rome.

Strack, K. M. (1992), *Exploration With Deep Transient Electromagnetics*, Elsevier Sci., Amsterdam.

Strack, K.-M., and K. Vozoff (1996), Integrating long-offset transient electromagnetics (LOTEM) with seismics in an exploration environment, *Geophys. Prospect.*, *44*(6), 997–1017.

Strack, K.-M., S. Dasgupta, S. Ellingsrud, and G. Yu (2009), Full field reservoir surveillance using electromagnetics, paper presented at European Association of Geoscientits and Engineers Annual Meeting, Workshop W2, Amsterdam.

Tabbagh, A. (1985), The response of a three-dimensional magnetic and conductive body in shallow depth electromagnetic prospecting, *Geophys. J. R. Astron. Soc.*, *81*(1), 215–230.

Wait, J. (1966), Fields of a horizontal dipole over a stratified anisotropic half-space, *IEEE Trans. Antennas Propag.*, *14*(6), 790–792.

Wang, Z., W. K. Hirschet, and G. Sedgwick (1991), Seismic monitoring of water floods?—A petrophysical study, *Geophysics*, *56*(10), 1614–1623, doi:10.1190/1.1442972.

Wannamaker, P. E., G. W. Hohmann, and W. A. Sanfilipo (1984), Electromagnetic modeling of three-dimensional bodies in layered earths using integral equations, *Geophysics*, *49*(1), 60–74.

Wirianto, M., W. Mulder, and E. Slob (2009), A study of land CSEM reservoir monitoring in a complex 3-D model, paper presented at European Association of Geoscientits and Engineers Annual Meeting, Amsterdam.

Wright, D., A. Ziolkowski, and B. Hobbs (2002), Hydrocarbon detection and monitoring with a multicomponent transient electromagnetic (MTEM) survey, *Leading Edge*, *21*(9), 852–864.

Wulff, A.-M., and S. Mjaaland (2002), Seismic monitoring of fluid fronts: An experimental study, *Geophysics*, *67*(1), 221–229, doi:10.1190/1.1451622.

Zhdanov, M. S. (2002), *Geophysical Inverse Theory and Regularization Problems*, Elsevier, Amsterdam.

Zhdanov, M. S., V. I. Dmitriev, S. Fang, and G. Hursan (2000a), Quasi-analytical approximations and series in electromagnetic modeling, *Geophysics*, *65*(6), 1746–1757.

Zhdanov, M. S., S. Fang, and G. Hursan (2000b), Electromagnetic inversion using quasi-linear approximation, *Geophysics*, *65*(5), 1501–1513.

Zhdanov, M. S., S. K. Lee, and K. Yoshioka (2006), Integral equation method for 3-D modeling of electromagnetic fields in complex structures with inhomogeneous background conductivity, *Geophysics*, *71*(6), G333–G345.

F. Rejiba, C. Schamper, and A. Tabbagh, UMR 7619 Sisyphe, University Pierre and Marie Curie, 4 pl. Jussieu, Case 105, F-75005 Paris, France. (faycal.rejiba@upmc.fr; cyril.schamper@upmc.fr; alain.tabbagh@upmc.fr)

S. Spitz, CGGVeritas, 1 rue Léon Migaux, F-91300 Massy-Palaiseau, France. (simon.spitz@cggveritas.com)